COMPOSITION, STRUCTURAL AND MATERIAL PROPERTIES OF LEECH TEETH – EXAMPLE OF BIOINSPIRATION IN MATERIALS RESEARCH

JOSEF ŠEPITKA[a], JAROSLAV LUKEŠ[a], ONDŘEJ JIROUŠEK[b], DANIEL KYTÝŘ[b], and JAROSLAV VALACH[b]

[a] *Czech Technical University in Prague, Faculty of Mechanical Engineering, Technická 4, 166 07 Prague 6,* [b] *Institute of Theoretical and Applied Mechanics, Academy of Sciences of the Czech Republic, v.v.i., Prosecká 76, 190 00 Prague 9, Czech Republic*
Josef.Sepitka@fsid.cvut.cz

Keywords: bioinspiration, atomic spectroscopy, nanoindentation

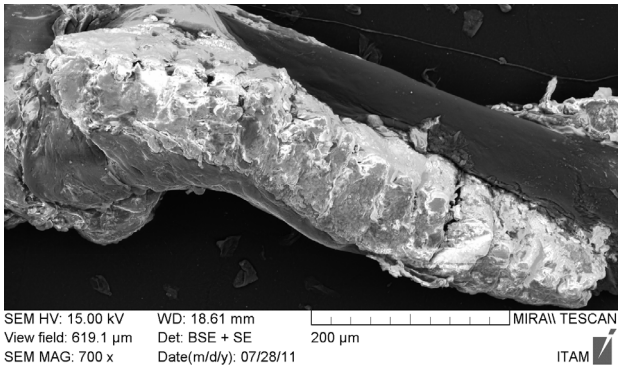

Fig. 1. **Top view on extracted leech's jaw with teeth line obtained by SEM with 700× magnification**

1. Introduction

The leech's sucking apparatus is an amazing instrument – it has 3 jaws and 300 teeth made for easily cut into the skin of the host animal. In ancient India and Greece, leeches have been used in medicine to remove blood from patients. Today, leeching is used rarely and the use of leeches has shifted into reconstructive and plastic surgery. Although there are a number of papers dealing with the leech stretch receptors, body wall muscles[1] or central nervous system CNS[2], there is no paper on the composition or material properties of its teeth. In this study we used nanoindentation and atomic spectroscopy to reveal composition and material properties of leech teeth and to demonstrate the optimization possibilities of nature to manufacture these very sharp and tiny blades which can easily penetrate the host's skin.

2. Experimental details

2.1. Sample extraction and preparation

Five samples of leech's jaws were obtained from adult subjects of *Hemopis sanguisuga*. The subjects were euthanised with ether and sliced in area of sucking apparatus. Individual jaws with length around 500 µm (depicted in Fig. 1) were carefully separated under magnification glass (5×) using a sharp-tip scalpel, microretractores and pair of tweezers. The samples were cleaned from the soft tissues and embedded in low shrinkage epoxy resin.

The surface of the samples was grinded and polished. Diamond grinding discs followed by monocrystalline diamond suspension were used for grinding procedure[3]. The best reached final surface roughness average (R_a) was 16 nm. All samples were prepared with roughness less than 40 nm, which is adequate value for micromechanical testing.

2.2. Mechanical testing

Quasi-static nanoindentation was performed using the nanomechanical instrument Hysitron TI 950 TriboIndenter™. Berkovich diamond tip, (triangular pyramids with angle of 142.3°) was used to obtain elastic properties of the teeth. The test was performed in three segments. Loading, constant force, unloading phase of the test were prescribed. Maximum force was reached at 5 s, then 2 s of dwell and 5 s of unloading followed.

The first set of 5 indents were performed on the sample with roughness approximately R_a = 40 nm. To reduce the influence of roughness on results, a force of P_{max} = 8000–8300 µN was applied resulting in indents depth app. 500 nm. Then the sample was polished again to

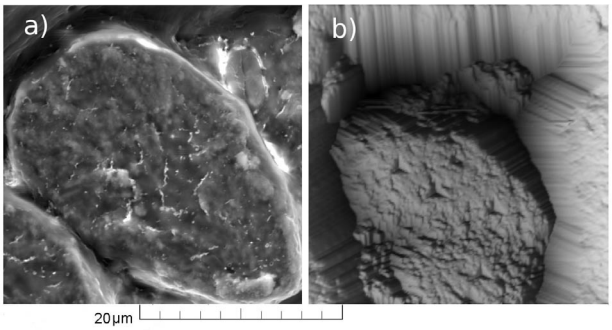

Fig. 2. **Detail of tooth (a) obtained by SEM with 8000x magnification (b) surface reconstruction with indents obtained by scanning probe microscopy (SPM) of image size 40×40 µm**

decrease its roughness down to R_a = 16 nm. The force of P_{max} = 900 μN corresponding to $h_{max} \approx$ 150 nm was used at this time. The force-depth curves were plotted for each indent, and reduced moduli were calculated using the Oliver-Pharr method[4].

2.3. Composition analysis

Morphological investigation of leech's teeth depicting its true size and shape has been accompanied with composition microanalysis. The microanalysis was carried out by Bruker Quantax energy dispersive spectrometer installed in Tescan MIRA II scanning electron microscope (SEM). Concentration of individual elements was determined from the relative intensity of their characteristic X-ray spectra by the Esprit program provided by microanalyser manufacturer. By the nature of elemental microanalysis it is impossible to identify molecular composition of the studied matter, only elemental composition is as the result available. From the composition analysis as the significant elements and their respective concentrations are calcium, oxygen and carbon were identified.

3. Results

In this preliminary analysis, the main constituents of leeche teeth have been identified. The tooth is composed mainly of calcium (41.9 %), oxygen (41.2 %) and carbon (11.4 %), other constituents are present in small quantities (F 2.1 %, Na 1.0 %, P 0.9 %, S 0.6 % and Mg 0.6 %). Therefore, a substance typical for mineral component in bones, hydroxyapatite is likely present in the teeth among other substances.

The mechanical properties of two leech teeth were measured in cross-section (depicted in Fig. 2). The average value of reduced modulus E_r = 29.41±1.10 GPa was obtained from 5 indents of the first test ($h_{max} \approx$ 500 nm, R_a = 40 nm). In the next measurement of 10 indents, the average modulus was E_r = 27.02±4.03 GPa ($h_{max} \approx$ 150 nm, R_a = 16 nm). These values correspond to the values from measurements on cortical bone and tooth dentin[5].

4. Conclusions

From the results of the nanoindentation it could be concluded that the mechanical properties of leech's tooth are independent on indentation depth. High-precision surface preparation allows indenting in small depths with a high accuracy. Another advantage of an achievement of very low roughness can be seen in the possibility for the placement of more indents in the same area. Reduction of indent size is very desirable because of the tiny cross section of the tooth surface, which is smaller than 1000 μm^2.

Mechanical properties and composition microanalysis of the teeth corresponding to biomaterials such as cortical bone or dentin[5] offers the assumption that it is possible that the tooth surface could be composed of enamel, as it is at higher animal species. Therefore, it would be beneficial to prepare longitudinal cuts of leech's teeth, which would enable the indentation of superficial layer and inner part of the teeth. Assessment of mechanical properties from different anatomical parts could help to determine whether the outer layer is created by enamel, and whether the inner part is composed of dentin. Based on this information, an accurate constitutive material model can be created.

The research has been supported by the Grant Agency of the Czech Republic (grant No. P105/10/2305), Ministry of Education of the Czech Republic: Transdisciplinary research in Biomedical Engineering II. No. MSM 6840770012 and research plan of the Academy of Sciences of the Czech Republic AV0Z20710524.

REFERENCES

1. Blackshaw S. E: Comp. Biochem. Phys. A, *105*, 4 (1993).
2. Elliot E. J., Muller K. J.: Brain Res. *218*, 1–2 (1981).
3. Dudíková M., Kytýř D., Doktor T., Jiroušek O.: Chem. Listy *105*, S (2011).
4. Oliver W. C., Pharr G. M.: J. Mater. Res. *7*, 6 (1992).
5. Lewis G., Nyman J. S.: J. Biomed. Mater. Res. B *87B*, 1 (2008).

J. Šepitka[a], J. Lukeš[a], O. Jiroušek[b], D. Kytýř[b], and J. Valach[b] *([a] Czech Technical University in Prague, Faculty of Mechanical Engineering, Prague, [b] Institute of Theoretical and Applied Mechanics, Academy of Sciences of the Czech Republic, v.v.i., Prague, Czech Republic):*

Composition, Structural and Material Properties of Leech Teeth – Example of Bioinspiration in Materials Research

The leech's sucking apparatus is an amazing instrument – it has 3 jaws and 300 teeth made for easily cut into the skin of the host animal. In this study, we used nanoindentation and atomic spectroscopy to reveal composition and material properties of leech teeth. Five samples of leech jaws obtained from adult subjects of *Hemopis sanguisuga* were investigated. Main constituents of leech teeth have been identified. The tooth is composed mainly of calcium (41.9 %), oxygen (41.2 %) and carbon (11.4 %), other constituents are present in small quantities (F, Na, P and S), and therefore, a substance typical for mineral component in bones hydroxyapatite is likely present in the teeth among other substances. Material properties, which are independent on indentation depth, examined by nanoindentation provided average reduced modulus E_r=27.54±3.71 GPa.

NANOINDENTATION BASED MICROANALYSIS OF HENS' BONES

LIBOR SEVERA[a], JIŘÍ NĚMEČEK[b], LADISLAV MÁCHAL[a], JIŘÍ VOTAVA[a], and JAROSLAV BUCHAR[a]

[a] Mendel University in Brno, Faculty of Agronomy, Zemědělská 1, 613 00 Brno, [b] Czech Technical University in Prague, Faculty of Civil Engineering, Thákurova 7, 166 29 Praha 6, Czech Republic
jiri.nemecek@fsv.cvut.cz

Keywords: hen bone, micro-mechanical properties, nanoindentation, elastic constants

1. Introduction

Bone mechanical properties and the presence of fractures in laying hens are both a welfare and an economic concern for the poultry industry. The mechanical properties of the bone have significant importance, especially in understanding fracture behavior as a function of mineralization. If we can obtain an insight into the determinants of the bone strength, then better methods to monitor and select animals with abnormal bones can be identified. The composition of the bone tissue is extremely complex compared to most engineering composites[1]. The organization of the bone within a Haversian system consists of a central canal surrounded by concentric lamella. Lamellae are observed at the level of a light microscope. A number of attempts have been made to describe the biomechanical properties of the bone at this level[1], but this description does not go beyond the histological level. The mechanical properties of cortical bones (including some micromechanical aspects) were described and reviewed in classical work by Reilly and Burstein[2] already in 1974 and more recently by Mammone and Hudson[3]. If one considers the elements that comprise a bone at the molecular level, at which the collagenous matrix and hydroxyapatite crystals appear, then a more fundamental understanding may be achieved. The view that bone may be considered as a two-phase composite to explain its mechanical properties was firstly suggested by Currey[4] back in 1964.

Concerning hens' bones (and similarly eggshells), different aspects such as genetic components[5], diet[6], breeding conditions[7] and/or hen breed[8] were monitored as determining factors. The differences between individual birds in terms of e.g. bone fracture incidence can not be explained by a sole factor. Differences can occur due to calcium metabolism, bone structure, or simply due to the body weight differences. A combination of factors is most likely involved[9]. Micro mechanical properties significantly affect the mechanical behaviour of the whole bone, as it was documented in number of works[10,11] and their detailed determination and interpratation is thus needed. One of the effective, precise and well-proven tools is the nanoindentation.

Nanoindentation has been previously used to compare the bone tissue properties in healthy bones with those of diseased and genetically modified small animal models (including mice, rats, and zebrafish)[12].

In nanoindentation, a small probe with nano-meter dimensions contacts a flat, prepared surface of a material. The resulting force and contact depth (i.e., displacement) data enable the calculation of elastic, plastic, and viscous material properties[13–15] of biological tissues like cortical or trabecular bones[16] or eggshells[17] at a spatial resolution similar to that of the tissue-level structural features in the bone. Nanoindentation can be also used to measure the creep behavior of biological tissues by fitting the depth vs. time data at constant load to rheological models[18]. Viscoelasticity may affect both the elastic and fracture characteristics of the bone[19,20].

In particular, nearly all of the nanoindentation studies on bio-tissues reported to-date employed the Oliver–Pharr method[13] to obtain elastic modulus and hardness values from the nanoindentation data. The basic assumption involved in this method is that the sample behaves purely elastically during unloading, but biological tissues such as bone are well-known to be viscoelastic in both the macroscopic level as well as the microstructural level[21]. Material viscoelastic effects during unloading are well-known to lead to erroneous results in the estimation of contact stiffness and area using the Oliver-Pharr method[13], and in the past, increasing the holding time before unloading and increasing the unloading rate have been suggested as effective procedures to reduce viscoelastic effects during unloading[20,22,23]. An alternative solution is to allow the viscoelastic effects to occur. But then a method that has been well established in monolithic engineering materials to correct for the viscoelastic effects should be used[24].

This study is focused on the use of nanoindentation as a tool for quantification the differences between micro mechanical properties of femoral cortical bone of healthy laying hen and laying hen with defective calcic metabolism.

2. Materials and methods

2.1. Hens' femoral bones

Two bone tissues were compared, both belonging to Rhode Island Red (RIR) laying hen, caged and fed in identical conditions in the breeding station in the Czech Re-

public. The birds were kept in the three-floor cage housing, with 650 cm^2 floor space of individual housing. One of the tissues was extracted from the cortical part of a femoral bone of clinically healthy hen (51 weeks old) with the incidence of cracked eggs lower than 2 % (further denoted as Healthy-series). The second one was extracted from the cortical part of a femoral bone of a hen with calcium metabolism defect (denoted as Ill-series). This defect was shown by a high presence of cracked eggs (more than 20 %).

2.2. Preparation of specimens

The bone specimens were dissected from the femoral diaphysis of a mature hen (RIR) and dried for 48 hours at room temperature. Effect of the bone drying and affecting the values of Young's modulus and hardness was documented for bovine bones[25] but not for hen's bones so far. The samples were milled down to a cylindrical shape of 10 mm in height, their main (cylindrical) axis being aligned with the longitudinal direction of the diaphysis. The specimens geometry and different stages of the testing procedure are shown in Fig. 1. After this preparatory step, the specimens were embedded into metacrylate tablet. The specimens were cold-prepared (the structure was not thermally affected). Commercially available two-component resin was used for metacrylate mixture preparation and the specimens were left to dry and cure for 8 hours. The tablets were polished in order to achieve flat surface with maximum roughness of 10–20 nm.

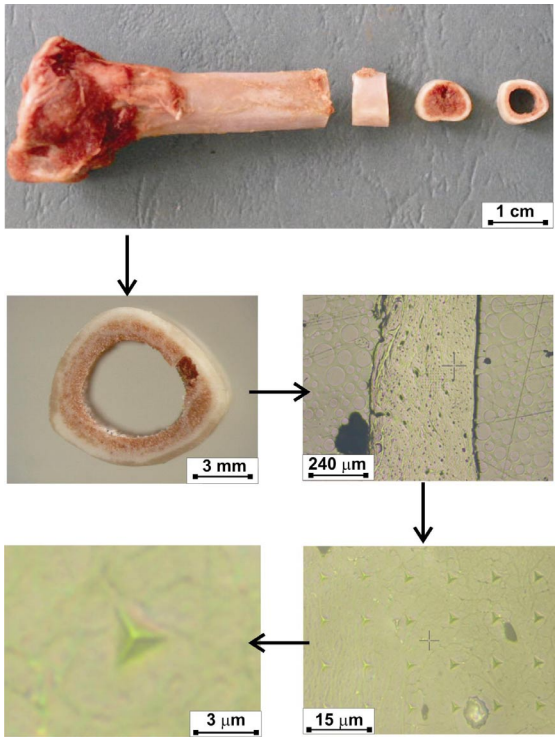

Fig. 1. **Preparation and testing of specimen in different scale levels**

2.3. Experimental set-up and loading conditions

The experiments were performed using nanohardness tester (CSM Instruments, Switzerland). A standard Berkovich tip was brought to the sample surface, producing a series of imprints. Influences of the tip geometry, contact depth, and contact area on nanoindentation properties of the bone were broadly discussed in literature[26], and the results were used for the configuration of presented experiments. The indenter has a nominal tip radius of $R \approx 50$ nm and a half-angle apex of $\theta = 65.27°$. The bone fragments were loaded in directions perpendicular to the cross-sections. Load vs. depth of penetration was measured throughout the whole procedure of loading, holding, and unloading. The load-controlled test was performed using the standard trapezoidal loading diagram as follows: linear loading (60 mN min^{-1}) up to the peak force (5 mN), then a 10 s holding period at the maximum force and linear unloading (60 mN min^{-1}) to zero force level (Fig. 2). Each sample cross-section was covered with a grid of 80 indents with 12 µm spacing. Similar experimental procedure and set-up was used e.g. by Severa et al.[17].

3. Results

Elastic modulus (E) and indentation hardness (H) were evaluated by standard procedure from unloading branches of a loading diagram[13] for each indent. Although, the elastic parameters show high scatter easily distinguishable decrease in both E and H can be observed for Ill-series as depicted in Figs. 3 and 4.

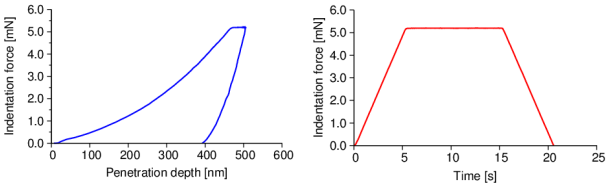

Fig. 2. **Example of a typical nanoindentation loading diagram**

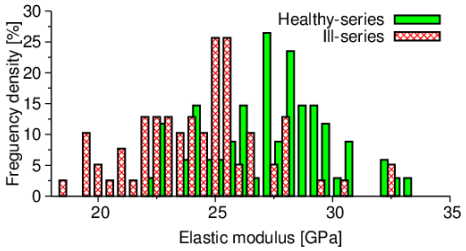

Fig. 3. **Histograms of elastic moduli for Healthy- and Ill-series**

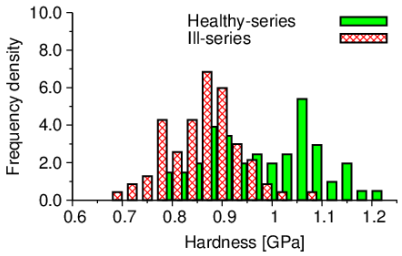

Fig. 4. **Histograms of indentation hardness for Healthy- and Ill-series**

The results of the performed experiments revealed that bone of a clinically healthy hen exhibited higher elastic modulus E and indentation hardness values H. It points to the fact that both elasticity and strength parameters (that are related to H) are afected in Ill-series. In case of non-defective tissue, following values were determined as: E=27.5±2.8 GPa, H=0.99±0.11 GPa, while in case of defective tissue as: E=24.5±3 GPa, H=0.88±0.07 GPa. Generally speaking, the values measured on the defective bone are approximately 11 % lower.

Based on optical microscopical observations, the healthy bone tissue contained larger pores in comparison with defective one. Interpretation of this fact needs much deeper investigation.

4. Discussion

This study utilised nanoindentation to investigate the mechanical properties of the microstructure of bone from the mid-femoral diaphyses of healthy and defective laying hen. Unlike the more conventional microhardness techniques, nanoindentation provides both modulus of elasticity and hardness estimates for a material and can be used to target specifically various bone tissue structures at a microscopic level.

A strong motivation behind the use of nanoindentation is the potential to understand the mechanical competence of a whole bone in the light of the properties of its structural units (osteons and trabecular packets) that result from the ongoing remodeling activity. However, given the prohibitively wide range of elastic data measured using bending, buckling, tensile, ultrasound tests or calculated using inverse numerical techniques[27], it still remains unclear how the indentation modulus can be converted into the elastic response of the bone tissue measured at higher levels of its hierarchical organization[28,29].

In general, the variations that have been recorded in the elastic modulus at the bone matrix level are rather high. The elastic modulus ranged between 22 and 38 GPa in osteonal bone of healthy hen and 16 and 32 GPa in osteonal bone of defective hen. The large scatter in E (as well as H) can be attributed mainly to the naturally varying crystalographic orientations within the cross section of the bone (differently oriented anizotropic lamelas and its fibers)[28,29]. The shape of the E and H histograms shows also on some kind of bimodality in the case of Healty-series which could be related to the prefferential collagen fiber orientations in the tested area. Despite this fact, presented study was focused on the evaluation of average properties in one direction only to give overall insight into the problem. More detailed research is planned in the future.

5. Conclusions

In the current study the differences between healthy and defect cortical bone tissues were documented and analysed in an average sense. Elastic modulus and hardness droped down by ~11 % for defected series. Similar approaches as used for studying human bones were employed. The data revealed and confirmed the fact that mechanisms described for human tissues can be largely adopted and used for detailed further research of hens' bones as well.

The research has been supported by the Grant Agency of the Czech Academy of Sciences under Contract No. IAA201990701 and Ministry of Education of the Czech Republic (Research Plan MSM 6840770003).

REFERENCES

1. Ascenzi A.: J. Biomech. Eng. *110*, 357 (1988).
2. Reilly D. T, Burstein A. H.: J. Bone and Joint Surgery *56*, 1001 (1974).
3. Mammone J. F., Hudson S. M.: J. Biomech. *26*, 439 (1993).
4. Currey J. D.: Biorheology *2*, l (1964).
5. Bishop S. C., Fleming R. H., McCormack H. A., Flock D. K., Whitehead C. C.: British Poultry Sci. *41*, 33 (2000).
6. Lichovníková M., Zeman L., Jandásek J.: Czech J. Animal Sci. *53*, 7 (2008).
7. Lichovníková M., Zeman L.: Czech J. Animal Sci. *53*, 162 (2008).
8. Máchal L., Jeřábek S., Zatloukal M., Straková E.: Czech J. Animal Sci. *49(2)*, 51 (2004).
9. Clark W. D., Cox W. R., Silversides F. G.: Poultry Sci. *87*, 1964 (2008).
10. Hengsbergera S., Enstroema J., Peyrinb F., Zysset Ph.: J. Biomech. *36*, 1503 (2003).
11. Baranová D., Pešek L., Sály J.: Folia Veterinaria *52*, 168 (2008).
12. Ebenstein D. M., Pruitt L. A.: Nano Today *1*, 26 (2006).
13. Oliver W. C., Pharr G. M.: J. Mater. Res. *7*, 1564 (1992).
14. Oyen, M. L., Cook, R. F.: J. Mater. Res. *18*, 139 (2003).
15. Olesiak S. E., Oyen M. L., Ferguson V. L.: Mechanics of Time-Dependent Mater. *14*, 111 (2010).
16. Jiroušek O. et al.: Chem. Listy *105* (*S*) (2010).
17. Severa L., Němeček J., Nedomová Š., Buchar J.: J.

Food Eng. *101*, 146 (2010).
18. Menčík J., He L. H., Němeček J.: Polymer Testing *30*, 101 (2010).
19. Němeček J.: Mater. Charact *60*, 1028 (2009).
20. Wu Z., Baker T. A, Ovaert T. C, Niebur G. L.: J. Biomech., *in press* (2011).
21. Wang, X. M., Cui F. Z., Ge J., Zhang Y., Ma C.: Biomaterials *23*, 4557 (2002).
22. Cheng Y. T., Ni W. Y., Cheng C. M.: J. Mater. Res. *20*, 3061 (2005).
23. Bushby A. J., Ferguson V. L., Boyde A.: J. Mater. Res. *19*, 249 (2004).
24. Tang B., Ngan A. H. W., Lu W. W.: J. Mater. Sci.: Mater. Medicine *18*, 1875 (2007).
25. Rho J. Y., Pharr G. M.: J. Mater. Sci.: Mater. Medicine *10*, 485 (1999).
26. Paietta R. C., Campbell S. E, Ferguson V. L.: J. Biomech. *44*, 285 (2011).
27. Guo X. E.: *Mechanical properties of cortical bone and cancellous bone tissue*. In: (Cowin S., ed.)), Bone Mechanics Handbook, 2nd Edition. CRC Press, Boca Raton 2000.
28. Hengsberger S., Enstroem J., Peyrin F., Zysset P. K.: J. Biomech. *36*, 1503 (2003).
29. Zysset P. K.: Osteoporosis Int. *20*, 1049 (2009).

L. Severa[a], J. Němeček[b], L. Máchal[a], J. Votava[a], and J. Buchar[a] *([a]MENDELU, Brno, [b]CTU in Prague, Czech Republic):* **Nanoindentation Based Microanalysis of Hens' Bones**

The research is focused on the use of nanoindentation as a tool for quantification of the differences between micro mechanical properties of femoral cortical bone of healthy laying hen and laying hen with defective calcic metabolism. In general, the variations that were recorded in the elastic modulus at the bone matrix level are rather high. The elastic modulus ranged between 22 and 38 GPa in osteonal bone of healthy hen and 16 and 32 GPa in osteonal bone of defective hen. The shape of the *E* and *H* histograms shows also some kind of bimodality, which can be related to prefferential collagen fiber orientations in the tested area.

MICROSTRUCTURE CHARACTERISTICS OF Fe-0.85Mo-3Mn-0.5C SINTERED STEEL IN DEPENDENCE ON SINTERING CONDITIONS

VLADIMÍR SIMKULET, and ĽUDOVÍT PARILÁK

Faculty of Manufacturing Technologies of the Technical University of Kosice with a seat in Presov, Bayerova 1, 080 01 Presov, Slovak Republic
vladimír.simkulet@tuke.sk

Keywords: powder metallurgy, alloying, microhardness measurement

1. Introduction

The development of new alloys, based on composition containing Mn with possible addition of Mo, is an important attempt to increase the application of different sintering processes, especially when special use are required. Moreover, the presence of Mn and Mo as alloying elements is very important; in fact they are helpful to improve hardenability and the mechanical properties[1–7]. However, due to the high dew point, Mn oxides are not reduced during the sintering cycle at atmosphere with dew point approximately –25 °C, accordingly Mn had been avoided, in the past, in ferrous powder metallurgy[8]. The problem of oxide network formation in PM steels with different Mn contents was investigated in ref.[9]. The paper describes local mechanical properties evaluated by microhardness measurement and alloying process after difference sintering conditions. Microhardness was measured in the due zone, in core of iron particles and measured in thick alloyed surface layer. Vickers microhardness test was evaluated on metallographic cross-sections according to STN EN ISO 6507, testing equipment Leco LM 700 with weight 25 g.

2. Experimental procedure

The following powders were used for the preparation of the samples:

- prealloyed Astaloy85Mo powder (Höganäs AB),
- atomized ASC100.29 powder (Höganäs AB),
- Manganese in form of medium carbon ferromanganese (80 % Mn, 1.1 % C, particle size < 45 μm, 0.67 % O, milled in air, EratemElkem),
- Natural graphite CR12 (Grafit Netolice).

The powders were mixed as two systems:
A) Fe – 0.85 % Mo – 3 % Mn – 0.5 % C (referred to as A)
B) Fe – 3 % Mn – 0,5 % C (referred to as B), both were prepared with 0.8 % HW wax as lubricant. The samples (ø 10 × 10 mm) made of the mixed powders compacted at 600 MPa were sintered in dissociated ammonia (dew point –30 °C) at 875 °C, 1120 °C and at 1200 °C for 1, 3, 5, 10, 30 and 60 min in a Mars furnace.

3. Results and discussion

The aim was the comparison of microstructure creation for iron and molybdenum powders independence on manganese addition at chosen sintering conditions, i.e. ferrous matrix alloyed by molybdenum and matrix without molybdenum alloying. Microstructure of samples for both systems A and B was covered after sintering for 1 min with a thin manganese alloying layer as a result of sublimation and condensation of manganese vapors. Centres of the particles remain ferritic. In the case of sintering time at 3 min, Fig. 1a, the matrix was alloyed by manganese along grain boundary – intensive bounders (diffusion to be at grain boundary faster than in a volume). It came to further highlight of grain boundaries and partly to alloying of centers of powder particles after sintering within 5 min. Character of microstructure samples of system B after sintering 30 min corresponds approximately to microstructure samples according to Fig. 1b. In system A sintered at 1120 °C during 1 min we observe more expressive alloying only on particles surface. On the other side system B alloying of core particles by manganese is more intensive at grain boundaries. This shows that the diffusion of manganese from surface was quicker due to higher sintering temperature in molybdenum alloyed matrix. Microstructure of this system was heterogeneous, but evidently different. Alloying of matrix extends in both systems after sintering for 3 min at sintering 1120 °C, but more in molybdenum alloyed.

After sintering at 1200 °C perhaps equal behavior of alloying matrix is observed but only with the difference that a higher homogeneity value of microstructure was achieved. Microstructure of system A evidently consists of bainite and manganese supports bainite formation especially after sintering at 1200 °C for 60 min.

Microhardness values for both systems are described in Fig. 2. Higher microhardness volumes were in samples

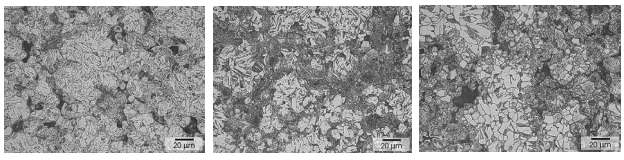

a b c

Fig. 1. **Sintering after 875 °C a) system A during sintering time 3 min, b) system B during sintering time 5 min, c) system B during sintering time 30 min**

prealloyed by molybdenum, Fig. 2a. Microhardness of edges particles at samples of B system after sintering at 875 °C was possible measured during sintering for 30 min only. This also shows the slower diffusion of manganese in iron matrix. It is clear that microhardness values were also affected by carbon in border areas. The microhardness values of microstructure samples sintered at 1120 °C are shown in Fig. 2b. This diagram evidently shows continuous increase of microhardness at borders and small change of microhardness in centre of elements systems. On basis of high microhardness value it can be expected that in border of manganese alloyed areas carbides type of (Fe-, Mo-, Mn-) C were created. The microhardness values of both types of samples after sintering at 1200 °C are shown in Fig. 2c. These microhardness values again show the molybdenum prealloyed matrix as uniform and more hardened, which can be caused as we already mentioned by carbides formation. Microhardness of grain borders corresponds to a martensite after longer sintering time.

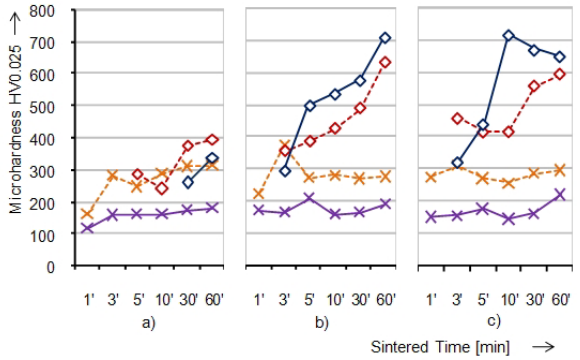

Fig. 2. **Microhardness values (HV0.025) of sintered systems. a) sintered after 875 °C, b) sintered after 1120 °C, c) sintered after 1200 °C.** Legend:

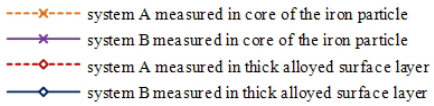

4. Conclusions

Following main results were obtained: Mo alloyed and Fe matrix of compacts samples are alloyed by manganese already at low temperature and apparently during a 3 min. By extension of sintering time and by higher sintering temperature the alloying process of matrix by manganese is reflected by the alloying of powder elements inside and by bigger or smaller homogeneity. We have found out in molybdenum alloyed matrix a more uniform alloying by manganese, which was demonstrated by higher microhardness values. Ferritic grains were located in iron matrix after longest sintering time and at higher sintering temperature. Microstructure of investigation material on bases of prealloyed powder affected by manganese comprised mainly bainite and the grains of ferrite occurred in microstructure of mixed system under all sintering condition.

Authors thank for supporting this research by structural funds of EU grant with ITMS 26220220125 of Agency of Ministry of education of Slovak Republic.

REFERENCES

1. Bidulský R., Grande M. A., Kabatová M.: Chem. Listy *105*, s14 (2008).
2. Šalak A., Vasilko K., Selecká M., Danninger H., Jakubéczyová D., Fáberová M.: Proc. DFPM (2005).
3. Kupková M., Kupka M., Strobl S., Hvizdoš P.: Chem. Listy *105*, s17 (2010).
4. Zubko P., Pešek L., Bláhová O.: Chem. Listy *105*, s17 (2010).
5. Matija R., Vojtko I.: Proc. Progressive Methods of Machining (2011).
6. Novák-Marcinčin J., Barna J., Nováková-Marcinčínová Ľ., Fečová V.: Tehnički Vjesnik *18*, 4 (2011).
7. Duszová A., Horňák P., Stoyka V., Hvizdoš P., Lofaj F., Dusza J.: Chem. Listy *105*, s17 (2011).
8. Castro F., García W., Sainz S.: World Congress on Powder Metallurgy and Particulate Mat. (2008).
9. Selecká M., Keresti R., Šalak A., Bureš R.: Acta Metallurgica Slovaca *7*, 1 (2001).

V. Simkulet, and Ľ. Parilák *(Faculty of Manufacturing Technologies of the Technical University of Košice with a seat in Prešov, Slovakia):* **Microstructures Characteristics of Fe-0.85Mo-3Mn-0.5C Sintered Steel in Dependence on Sintering Conditions**

Manganese in combination with Molybdenum atomized prealloyed powder forms a new group of sintered high strength steels. The final properties of these steels depend on microstructure homogeneity. The aim was to investigate the alloying of molybdenum prealloyed powder with manganese in comparison with plain iron powder. The circular cross section samples were prepared for the investigation from basis water atomized and plain iron powders. The microstructure characteristics of sintered samples were characterized by micro hardness measurement.

COMPARISION OF MECHANICAL PROPERTIES OF NITRIDED CASES AND REMELTED LAYERS OF AUSTENITIC STAINLESS STEEL

ARTUR SITKO, MAREK SZKODO, and BEATA ŚNIEGOCKA

University of Technology in Gdańsk, Faculty of Mechanical Engineering, Department of Materials and Welding Engineering, ul. Gabriela Narutowicza 11/12, 80-233 Gdańsk
asitko@mech.pg.gda.pl

Keywords: remelted layer, nitrided layer, austenitic stainless steel, diffusion layer, termochemical treatment, glow-discharge nitriding process, nanohardness

1. Instroduction

The austenitic stainless steels have very high general corrosion resistance, but they have low hardness and wear resistance. Nowadays, material technologies like laser remelting and low-temperature glow-discharge nitriding process can improve mechanical properties of austentic stainless steel without decrease the corrosion resistance. Laser remelting influence on refinement of microstructure and homogenizing of chemical composition of alloys was studied in ref[1–4]. If the austenitic stainless steels are subjected to glow-discharge nitriding prosess in low temperature, loss of corrosion resistance is not observed. At the temperatures above 450 °C, the precipitation of CrN was observed. The limiting temperature of nitriding process could be about 450 °C, according to the[5–8].

The aim of this article is an analyse of local mechanical properties of nitrided cases and remelted layers after the low temperature glow-discharge nitriding process and laser remelting, respectively.

2. Experimental procedures and results

Every test specimens (diameter of 20 mm and height of 6 mm) were made of austenitic stainless steel type X5CrNi18-10. Young's modulus of the steel substrate is approximetely 200±14 GPa and its hardness is about 220±3 HV20. The specimens were subjected to glow-discharge nitriding process at the temperature of 450 °C. Chemical composition of gas mixture during the termochemical treatment was different. Parameters of nitriding process are shown in Tab. I.

The same steel type X5CrNi18-10 was subjected to laser remelting. Laser remelting was done by means of laser MLT 2500 CO_2 (wavelength 10.6 μm) in argon atmosphere. During the laser remelting process no. 5 and 6 the specimens were also immersed in liquid nitrogen. The laser beam dimension 1×20 mm was used. Tab. II presents parametres of laser treatment.

Table I
Parametres of the glow-discharge nitriding process

Number of process	Vacuum pressure [hPa]	Time [h]	Temperature [°C]	Atmospheric composition	
				N_2	H_2
1	4	6	450	10	90
2	4	6	450	50	50

Representative picture of remelted layers is presented in Fig. 1. After laser remelting the surfaces were grinded off through 1200 grit SiC papers. The depth of the remelted layers depended on the laser power. Generally, the increase of the power caused a rise of thickness of the remelted layers.

Investigation of mechanical properties was carried out by using hardness tester with mounted Berkovich indenter. Mechanical properties of the diffusion layers were

Table II
Parametres of the laser remelting

Number of process	Scanning velocity [m min^{-1}]	Power [kW]	Scanning velocity [m min^{-1}]
3	2	2	0,25
4	2	5	0.25
5	2	2	0.25
6	2	5	0.25

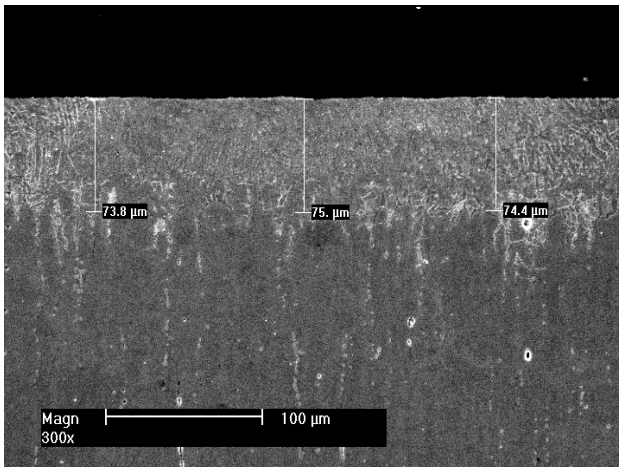

Fig. 1. **Microstructure of remelted layer after process laser remelting**

Table III
Mechanical properties of nitrided and remelted layers

Process	Nano hardness [HV]	Young's modulus [GPa]	Load [mN]
1	614±55	211±28	10
	524±71	201±19	20
	465±44	187±16	30
2	1056±13	232±28	10
	861±98	228±19	20
	737±59	198±18	30
3	352±32	227±17	10
	337±36	213±18	20
	327±22	192±16	30
4	412±42	235±21	10
	411±38	206±18	20
	330±22	192±19	30
5	432±67	227±23	10
	394±42	213±21	20
	377±43	192±17	30
6	432±54	235±26	10
	400±43	206±20	20
	368±32	192±14	30

examined on the surface of specimens using a different loads. Results of surface hardness were obtained by using different loads, respectively: 10, 20, 30 mN. Research was done by means of CSEM NanoHardnessTester (NHT) produced in Switzerland. Oliver-Pharr method was used for calculation of modulus. The value of Poisson's ratio was 0.3. Nanohardness was automatically recalculated between scales and presented in Vickers hardness scale. The results are shown in Tab. III.

3. Conclusion

1. Glow-discharge nitriding process has beneficial influence on nanohardness and Young's modulus.
2. The increase of nitrogen content in gas mixture influence on higher value of Young's modulus.
3. Laser remelting caused the refinement of microstructure in obtained surface layer.
4. Laser remelting process has beneficial influence on nanohardness and Young's modulus.

REFERENCES

1. Pan Q., Huang W., Song R., Zhou Y., Zhang G.: Surf. Coat. Technol. *102*, 245 (1998).
2. Khalfallah I., Rahoma M., Abboud J , Benyounis K.: Optics & Laser Technol. *43*, 806 (2011).
3. Kwok C., Man H., Cheng F.: Surf. Coat. Technol. *99*, 295 (1998).
4. Kwok C., Lo K., Chan W., Cheng F., Man H.: Corros. Sci. *53*, 1581 (2011).
5. F. Borgioli, A. Fossati, G. Matassini, E. Galvanetto, T. Bacci: Surf. Coat. Technol. *204*, 3410 (2010).
6. Köster K., Kaestner P., Bräuer G., Hoche H., Troßmann T., Oechsner M.: Surf. Coat. Technol. doi:10.1016/j.surfcoat.2011.10.059 (2011).
7. Li Y., Wang L., Xu J., Zhang D.: Surf. Coat. Technol. *206*, 2430 (2012).
8. Liang W., Xiaolei X., Zhiwei Y., Zukun H.: Surf. Coat. Technol. *124*, 93 (2000).
9. Liang W., Juncai S., Xiaolei X.: Surf. Coat. Technol. *145*, 31 (2001).

A. Sitko, M. Szkodo, and B. Śniegocka *(University of Technology in Gdańsk, Faculty of Mechanical Engineering, Department of Materials and Welding Engineering, Poland):* **Comparison of Mechanical Properties of Nitrided Cases and Remelted Layers of Austenitic Stainless Steel**

This article presents the results of nanohardness and Young's modulus of nitrided cases and remelted layers. The nitrided cases were obtained by using the glow-discharge nitriding process at the temperature of 450 °C. The termochemical treatment was done by using a different chemical composition of gas mixture (N_2:H_2). The laser remelting was done by using the TRUMPF laser TLF 6000 turbo in Kielce. The laser remelting was done by using different parameters of termochemical treatment. Investigation of mechanical properties was carried out by using hardness tester with mounted Berkovich indenter. Mechanical properties of the diffusion and remelted layers were examined on the surface of specimens using different loads.

NANOINDENTATION TESTING OF LOW-ALLOYED MOLYBDENUM SINGLE CRYSTALS

KATEŘINA SKOTNICOVÁ[a], MICHAL VYLEŽÍK[b], VLASTIMIL MATĚJKA[c], and JAROMÍR DRÁPALA[a]

[a] *Department of Non-ferrous Metals, Refining and Recycling, VŠB – Technical University of Ostrava, Av. 17. listopadu 15, 708 33 Ostrava-Poruba,* [b] *Centre for Advanced Innovation Technology, Av. 17. listopadu 15, 708 33 Ostrava-Poruba,* [c] *CNT – Nanotechnology Centre, Av. 17. listopadu 15, 708 33 Ostrava-Poruba, Czech Republic*
Katerina.Skotnicova@vsb.cz

Keywords: nanoindentation, molybdenum alloy, single crystal, hardness, elastic modulus

1. Introduction

Nanoindentation methods are applied to study nano-scale material deformations and enable accurate measurements of indentation load (P) and penetration depth (h). Mechanical properties, Young´s modulus and hardness can be obtained from nanoindentation by numerical calculations of the load-displacement curves including loading and unloading process according to Oliver-Pharr method (ref.[1–4]). Recent research has shown that the hardness determined by nanoindentation depends on a test load, i.e. hardness at small depth is much greater than at greater depth. This phenomenon is called the Indentation Size Effect (ISE) (ref.[5,6]). Another method used to measure hardness from load-depth curves is work-of-indentation method. The total mechanical work of indentation can be determined by computing the area under the force increasing portion of the test force vs. indentation depth curve (ref.[7]). The total work includes two components: elastic and plastic. The elastic work can be obtain by the area under the force decreasing portion of the F vs. h curve, and the plastic work can be determine from the area between the force increasing and force decreasing curve.

Work of indentation method as a means of determining hardness was first proposed by Stillwell and Tabor (ref.[8]). The conventional representation of hardness, maximum applied load P divided by the residual area of indent impression A_p, is equivalent to the ratio of plastic work W_{pl} to the plastic deformed volume of the indent V_{pl} (ref.[7, 8]):

$$\frac{F}{A_F} = \frac{W_{pl}}{W_{el}} \qquad (1)$$

The total work W_t can be obtained by integrating loading curve:

$$W_t = \int_0^{h_{\max}} P(h)dh = \int_0^{h_{\max}} Ch^2 = \frac{P_{\max} h_{\max}}{3} \qquad (2)$$

For sharp indentation of elastic-plastic material, the loading response is governed by $P = Ch^2$. The ration h_f/h_{max} is equivalent to that of W_{pl}/W_t. The plastic work W_{pl} can be determined from Eq. (*3*):

$$\frac{W_{el}}{W_{pl}} = 1 - \frac{W_{pl}}{W_t} = 1 - \frac{h_f}{h_{\max}} \qquad (3)$$

where h_f is the final depth of contact impression after unloading and h_{max} the indenter depth at peak load. The hardness concerning total work of indentation, resp. plastic work of indentation can be calculated from Eq. (*4*) (ref.[9]), where κ is a constant equal to 0.0408 for the three sided Berkovich pyramidal indenter:

$$H_{Wt} = \frac{\kappa P_{\max}^3}{9W_t^2} \qquad \text{resp.} \quad H_{Wpl} = \frac{\kappa P_{\max}^3}{9W_{pl}^2} \qquad (4)$$

Atomic force microscopy (AFM) can be used for imaging of residual indentations and obtaining accurate dimensional information from an image area of only a few microns.

In this paper, the indentation hardness, Young´s modulus, total and plastic work of pure and low-alloyed molybdenum single crystals are investigated. We compare hardness from the Oliver and Pharr analysis (H_{IT}) and the work-of-indentation method described above. The influence of niobium as an alloying element and crystallographic orientation of single crystals on these nano-scale properties is studied. The effect of the load on pile-up formation is also investigated using AFM imaging.

2. Experimental

Bulk single crystals of Mo-2 wt.% Nb with crystallographic orientation <110> and <100> were used for the experiment. The pure molybdenum single crystal with crystallographic orientation <110> was included in the experiment due to a study of the influence of niobium on the mechanical properties of molybdenum single crystal. All single crystals were prepared by the electron beam zone melting (method of floating zone). The surface of specimens was polished using diamond pastes and *electrolytically in NaOH solution.* The indentation experiments were conducted with the standard three-sided pyramidal Berkovich tip using Triboindenter TI 950 (Hysitron). The tip radius was about 150 nm. For an easier interpretation of mechanical behaviour at various depth, the maximum load

was changed at intervals: 1000, 2000, 3000 and 4000 μN and then unloaded. The dwell time was 2 s. For each material, six indentations were made at each load and the presented results are averages for the group. These indentation loads corresponds to applied depths from 69 to 190 nm for all specimens. The topography of the selected indents was acquired using atomic force microscope SOLVER Next^{TM} (NT-MDT) operated in contact mode. The probes PPP-CONTR (Nanosensors) were used for imaging. The AFM images were processed using software Gwyddion (version 2.25).

3. Results and discussion

The load-depth curves for Mo-2 wt.% Nb <100> single crystal for all applied loads are given in Fig. 1 as an example.

The elastic recovery appears in load-depth curves during unloading processing for all specimens, but the elastic recovery of Mo-2 wt.% Nb with crystallographic orientation <100> is less than other specimens. Fig. 2 shows one of AFM 3D-images of indentations (load 4000 μN) for molybdenum-base single crystals. It is visible that edges of an indentation bend to center because of elastic recovery.

The hardness values H_{IT}, H_{Wt} and H_{Wp} of all specimens are plotted as a function of applied load in Fig. 3 to 5. The results display a strong size effect, i. e. the hardness decreases as the indentation load or indentation depth increases, which is commonly referred to as the indentation size effect (ISE). Numerous investigators have reported studies of ISE using nanoindentation testing for various materials (ref. [6,10,11]). The hardness values calculated using the plastic work of indentation are the highest, especially in smaller depth or for low applied loads. It was found that the hardness of all specimens estimated by the O-P method was significantly (up to 30 %) lower than the hardness calculated using the total work-of-indentation. There are only small differences between the values of hardness for both specimens of Mo-Nb single crystals with different crystallographic orientation. The plastic work must be less than total work, but the plastic hardness H_{Wpl} is larger than H_{Wt}.

The hardness values calculated from the work-of-indentation approach rise more steeply at lower applied load than the hardness values calculated by the O–P method. The reason of this effectcan be explained by the fact that the method of Tuck et al. (ref.[9]) makes no allowance for changes in tip geometry at lower indentation depths, where the tip geometry can significantly influence the calculated values, whereas tip geometry effects are allowed for in the O–P calculations.

At low loading, the indent behaviour of specimens is almost elastic deformation, increasing the Young´s modulus (E_{IT}) – Fig. 6. It was observed that the hardness and Young´s modulus of Mo-2 wt.% Nb single crystal with the

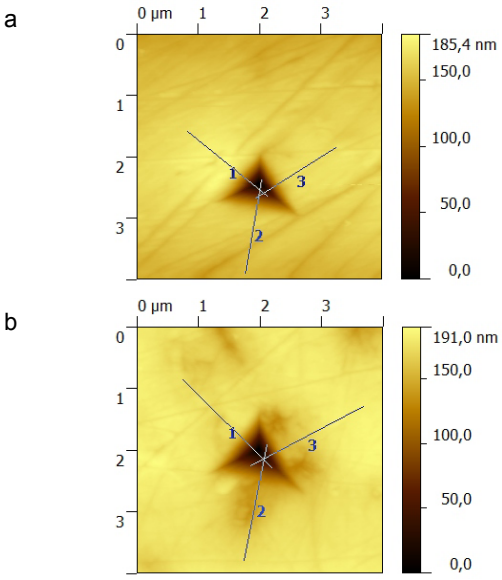

Fig. 2. **AFM images of Mo-Nb <110> (a) and Mo <110> (b) single crystals at load 4000 μm**

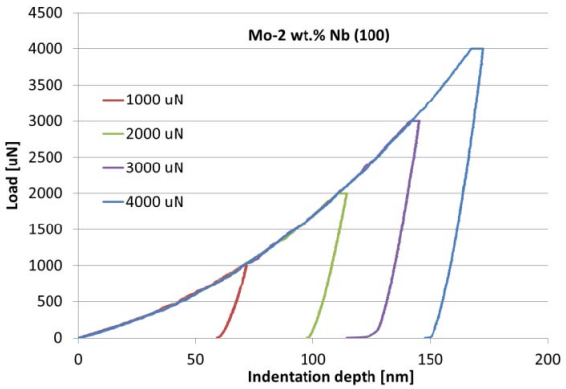

Fig. 1. **Load-depth curves of Mo-2 wt.% Nb <100> single crystal**

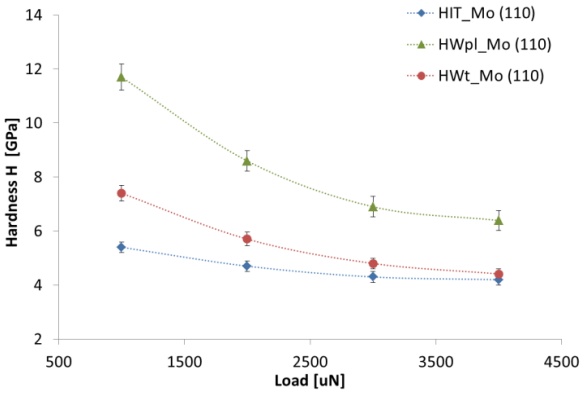

Fig. 3. **Comparison of hardness values obtained by two methods for pure Mo <110> single crystal**

orientation <100> increased at the indentation load 4000 μN probably results of the hardening effect (ref.[6]).

The contribution of the elastic work to total work decreases with increasing maximal load approx. from 21 to 17 % in the case of Mo-2 wt.% Nb and pure Mo single crystals with the orientation <110>. Because of the smaller elastic recovery for indentations into Mo-2 wt.% Nb <100>, there is lower differences between the total work of indentation approach and the plastic work of indentation approach – see Fig. 7.

There is the evident influence of crystallographic orientation of single crystals on mechanical properties. It is known that single crystals of molybdenum and its alloys show the anisotropy of mechanical properties, when the crystals with the crystallographic orientation <110> have much higher plasticity than these crystals with the crystallographic orientation <100> (ref.[12]). The Mo-Nb single crystal with orientation <100> has higher values of Young´s modulus and H_{IT} at most testing loads than adequate alloy with orientation <110>. The similar effect was observed in case of macro-scale testing of mechanical properties of Mo-Nb single crystals (ref.[12]). The alloying of molybdenum single crystal with niobium results in the increase of Young´s modulus and hardness.

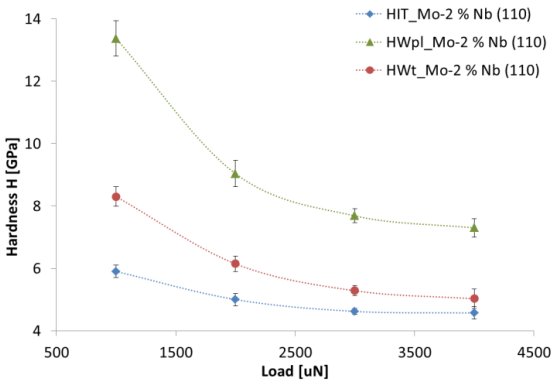

Fig. 4. **Comparison of hardness values obtained by two methods for Mo-2 wt.% Nb <110> single crystal**

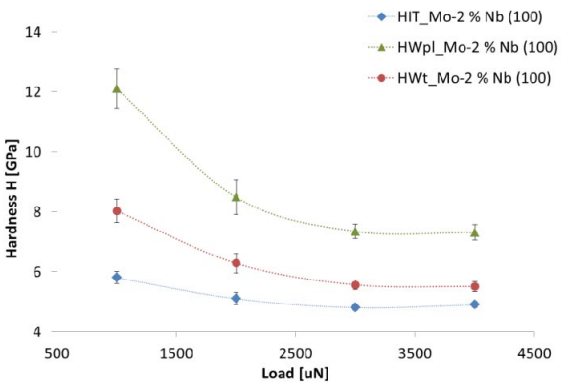

Fig. 5. **Comparison of hardness values obtained by two methods for Mo-2 wt.% Nb <100> single crystal**

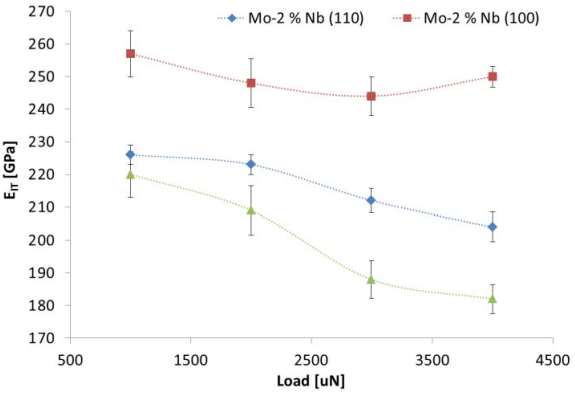

Fig. 6. **The load dependence of Young´s modulus for all single crystals**

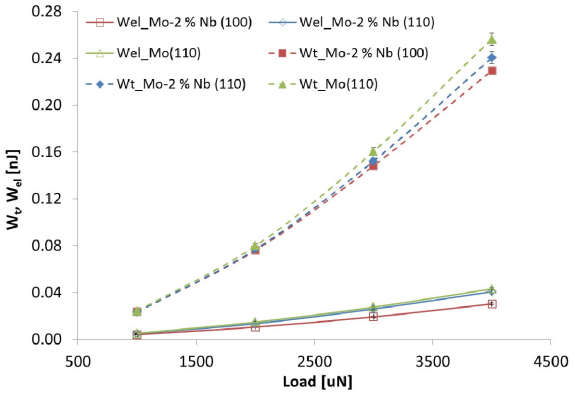

Fig. 7. **Work-depth curves for all single crystals**

The pile-up formation was visible in the AFM images of the indents only for Mo-2 wt.% Nb single crystal with orientation <100> (Fig. 8).

This result corresponds to findings by Stelmashenko et. al. (ref.[13]). In their study, the height of pile-ups on the (110) surface in molybdenum single crystal was very small for each of three different orientations of indenter, and there is no symmetry in the pile-up distribution.

4. Conclusions

The experiments and the above discussion yield the following results:

a) Under the same test condition, the nanohardness and Young´s modulus of all specimen declines as the load increases. The ISE of hardness values was observed.

b) The hardness estimated by the O-P method was significantly lower than the hardness calculated using the total work-of-indentation approach. The main advantage of work-of-indentation method is that there is no need to calculate the area of the indentation, which

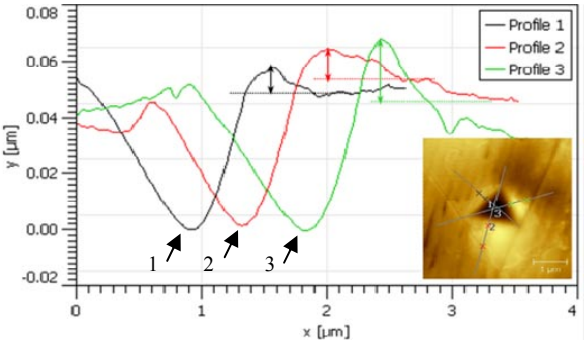

Fig. 8. **Height profile through an indentation (at 4000 mN) showing significant pile-up on the indentation edge in Mo-2 wt.% Nb <100>**

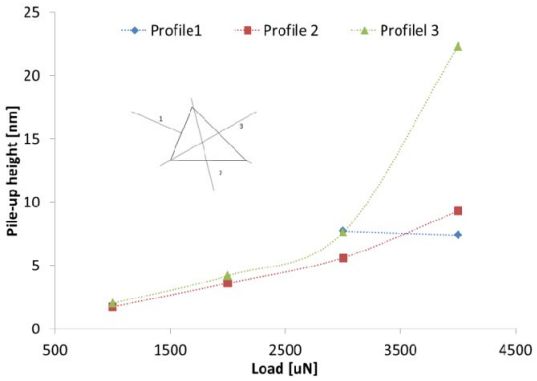

Fig. 9. **Plot of pile-up height with indentation depth in Mo-2 wt.% Nb <100>**

thus eliminates the problems caused by underestimating the contact area.

c) According to literature findings (ref.[12,13]), the hardness values should be higher for molybdenum-base single crystals with crystallographic orientation <100> than for these with crystallographic orientation <110>. The calculated H_{Wt} and H_{Wpl} values for the tested Mo-Nb single crystals don´t correspond to this fact. Thus the discrepancy of these hardness values must be examined.

d) Pile-up formation occurred at the edges of the indentations only in Mo-2 wt.% Nb single crystals with crystallographic orientation <100>. The widely used Oliver-Pharr model does not account for pile-up and consequently can overestimate hardness and elastic modulus.

e) It was confirmed that mechanical properties depend on the crystallographic orientations of single crystals. According to the results, the Mo-Nb single crystal with orientation <100> has higher values of E_{IT} than the same single crystal with orientation <110>. The alloying of molybdenum with niobium led to increasing of values of hardness and E_{IT}.

This work was elaborated in the frame of the research project MSM6198910013„Processes of preparation and properties of high purity and structurally defined special materials" and SP2011/170 "The anisotropy of micromechanical properties of selected type of steel".

REFERENCES

1. Oliver W. C., Pharr G. M.: J. Mater. Res. *7*, 1564 (1992).
2. Lucca D. A.: CIRP Ann-Manuf. Techn. *59*, *803* (2010).
3. Tricoteaux A., Duarte G., et al: Mech. Mater. *42*, 166 (2010).
4. Tabor D.: *The Hardness of Metals*. Clarendon Press, Oxford 1951.
5. Menčík J.: Chem. Listy. *105*, s115 (2011).
6. Voyiadjis G. Z., Peters R.: Acta. Mech. *211*, 131 (2010).
7. Beegana D., Chowdhury S., Laugier M. T.: Surf. Coat. Technol. *192*, 57 (2005).
8. Stilwell N. A., Tabor D.: Proc. Phys. Soc. *78*, 169 (1961).
9. Tuck J. R., Korsunsky A. M., et al.: Surf. Coat. Technol. *137*, 217 (2001).
10. Nix W. D. and Gao H.: J. Mech. Phys. Solids. *46*, 411 (1998).
11. Rashid K. Abu Al-Rub: Mech. Mater. 39 (2007).
12. Ljakišev N. P., Burchanov G. S.: *Metallic single crystals* (in Russian). ELIZ, Moskva 2002.
13. Stelmashenko N. A., et. al.: Acta Metal. Mater. *41*, 2856 (1993).

K. Skotnicová[a], M. Vyležík[b], V. Matějka[c], and J. Drápala[a] *([a] Department of Non-ferrous Metals, Refining and Recycling, VŠB – Technical University of Ostrava; [b] Centre for Advanced Innovation Technology, VŠB – Technical University of Ostrava; [c] CNT – Nanotechnology Centre, VŠB – Technical University of Ostrava, Czech Republic*): **Nanoindentation Testing of Low-Alloyed Molybdenum Single Crystals**

The indentation hardness, Young´s modulus, total and plastic work of pure and low-alloyed molybdenum single crystals were investigated. It was found that the hardness of specimens decreases as the indentation load or indentation depth increases due to the indentation size effect (ISE). The same trend was observed for the E_{IT} values of all specimens. The hardness estimated by the O-P method was significantly (up to 30 %) lower than the hardness determined using the total work-of-indentation approach. AFM 3D-images of indentations showed that pile-up formation occurred at the edges of the indentations only in Mo-2 wt.% Nb single crystals with crystallographic orientation <100>. It was confirmed that nanoscale mechanical properties depend on the crystallographic orientations of single crystals. The alloying of molybdenum with niobium led to increasing of values of hardness and E_{IT}.

INHOMOGENEOUS PLASTIC DEFORMATION OF TINPLATES UNDER UNIAXIAL STRESS STATE

EMIL SPIŠÁK, JÁN SLOTA, JANA MAJERNÍKOVÁ, ĽUBOŠ KAŠČÁK, and PETER MALEGA

Technical University of Košice, Letná 9, 042 00 Košice, Slovakia
emil.spisak@tuke.sk

Keywords: tinplate, plastic deformation, failure analysis

1. Introduction

Tinplate is essentially low carbon steel, cold reduced between 0.13 and 0.50 mm thick coated with tin produced for packaging industry. Modern tinplate possesses several important advantages, such as excellent drawability combined with good strength, good solderability and corrosion resistance. In many instances, special grades for specific can making techniques have been developed, e.g. for drawing and wall-ironing, redrawing and easy-open ends[1,2]. Their development has required close cooperation between packaging producers and tinplate manufacturers[3].

During the cold rolling on tandem mill the strength and hardness have been increased. On the other hand, the plastic properties of rolled materials have been decreased. To eliminate these negative changes in material, the recrystallization annealing is included in the sheet production process. Some products may be either batch annealed (BA) or continuously annealed (CA). Although the temper of the plate will be the same the mechanical properties may differ as CA plate has a finer grain structure (ref.[9,10]).

A number of materials exhibit discontinuous yielding under monotonic tension. A typical example is annealed mild steel. The monotonic stress–strain curve is not smooth but shows marked irregularities, with negative slopes occurring at or near the initial yield. Elastic deformation is terminated at a stress level known as the upper yield stress. Deformation proceeds at a decreased stress level known as the lower yield stress accompanied with inhomogeneous deformation. The specimen is divided into regions where the strain is relatively high (Lüders strain) and regions which are still elastic. The distinct plateau in the stress–strain curve is characterized by the propagation of Lüders bands. After the whole gage length has been strained by the amount of the Lüders strain, deformation becomes essentially homogeneous again[11].

The formation and propagation of Lüders bands in steels under tension are generally attributed to the strong interactions of interstitial atoms with dislocations, known as Cottrell atmospheres. In Cottrell atmospheres, interstitial atoms segregate to dislocations and pin them in position to lower the lattice distortion energy. At the upper yield stress, dislocations are unpinned from the Cottrell atmosphere and become free dislocations. These free dislocations can move at the lower yield stress and lead to multiplication of new dislocations. Therefore, during the propagation of Lüders bands, the elastic zones are essentially free of dislocations whereas Lüders bands have a high dislocation density. The upper yield stress is regarded as the nucleation stress, and the lower yield stress is the growth stress of the Lüders bands[4].

The macroscopic and microscopic characteristics associated with the propagation of Lüders bands under tension have been studied extensively. They include the angle and the propagation velocity of the Lüders fronts, the in-plane kinking of the strips, the influence of the number of Lüders fronts on the yield stress, and the strain profile at the Lüders fronts. Macroscopic shear bands can be readily observed at the front of the Lüders bands, and very often the band front makes a 45° angle with the loading axis. That is, the band front follows the plane of maximum shear stress. However, this is a first approximation. Some researchers (eg. ref.[7,12]) investigated some differences using specimens with specific cross-section or material, respectively.

The propagation of Lüders bands is influenced by many factors including crystal structure, grain size, composition and microstructure, shape and stiffness of the testing sample, strain rate, and the type of loading[13–15]. Grain size has a great influence on the Lüders strain and the morphology of the Lüders bands, particularly in the case for mild steels (eg. ref.[16]). The Lüders strain decreases significantly as the grain size increases. Zhang and Jiang[6] experimentally studied the local plastic deformation of a carbon steel subjected to monotonic tension. It was found that the strain at the Lüders front was lower than the full Lüders strain (the length of the plateau on the stress–strain curve). During the propagation of Lüders bands, the local deformation is inhomogeneous. The local strain was inhomogeneous even at the work-hardening stage.

In the paper, the BA and the CA double reduced tinplates for can making industry have been analysed. Inhomogeneous plastic deformation of DR tinplates under tension loading was experimentally studied.

2. Experiments

Tinplates are currently produced mainly two ways of rolling. Thicker steel sheets (0.18–0.30 mm) are produced by single reduction, after which the plates are continuous annealed. The sheets of smaller thickness (0.135–0.18 mm) are after the single reduction and annealing a second time rolled (double reduced – DR). Most of the current packaging sheets are further processed by

drawing (drawing two-pieces containers, lids, twist caps, etc.). For this reason, the thin sheets of packaging have to meet certain requirements on the mechanical and plastic properties. Compliance with mechanical properties that are mainly characterized by the yield stress and the tensile strength, it is currently difficult to achieve by the manufacturer within the required limits. Significantly greater problem is the plastic properties of thin metal packaging and method of their evaluation. At present the evaluation of thin sheets for packaging (in terms of standards) mainly the tensile test is used, but on the basis of supplier – customer relations are often used other tests (Springback test, Erichsen cupping test, Bulge test, and others). Based on past experience, the tensile test seems to be problematic for evaluation of thin steel packaging DR sheets[9,10].

In this work, a double reduced tinplates of TH550CA and TS550BA, respectively, with thicknesses of 0.17 mm were used for experiments. To determine an anisotropic properties of tested materials for the uniaxial tensile test samples in rolling direction 0° and perpendicular direction 90° in respect of rolling direction have been taken. From the uniaxial tensile test the following parameters have been evaluated: the yield stress, the ultimate tensile strength and total elongation.

The measured values are shown in Table 1. Typical chemical compositions for the tested materials are given in Table II.

Microstructures of the investigated steels in the direction of 0° and 90° are shown in Fig. 1 and Fig. 2. For both annealing processes of tested thin steel sheets the failure zones are shown in Fig. 3 and 4.

For these sheets that show Lüders band slip at uniaxial tensile test it is problematic to determine the value of maximum uniform deformation[10]. On tested samples it is showed a strain creation in specific sample sections. It

Table I
Mechanical properties of DR tinplates with thickness of 0.17 mm

Sample	Uniaxial test			Biaxial test		
	$Rp_{0,2}$ [MPa]	Rm [MPa]	A_{50} [%]	Re [MPa]	Rm [MPa]	A_B [%]
TS550BA⊥	442	434	3.7	509	598	4.4
TS550BA||	429	420	5.7			
TH550CA⊥	538	563	4.5	469	609	12.7
TH550CA||	579	591	10.5			

Table II
Chemical composition of experimental materials

Composition [%]	C	Mn	P	S	Si	Cu	Al	Cr
TS550BA	0.081	0.41	0.018	0.003	0.006	0.041	0.04	0.02
TH550CA	0.055	0.17	0.018	0.002	0.008	0.036	0.05	0.02

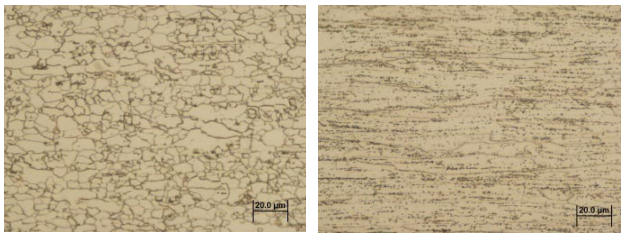

Fig. 1. **Microstructure of TH550CA (left) and TS550BA tinplates (right), direction 0°**

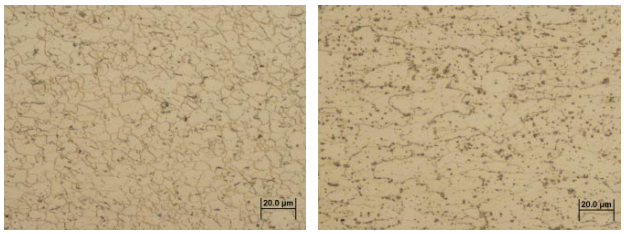

Fig. 2. **Microstructure of TH550CA (left) and TS550BA tinplates (right), direction 90°**

starts in one place, suddenly stops and passes into a completely different sample place (see Fig. 4). During the propagation of Lüders bands, multiple Lüders fronts can be formed. Under tension with a constant axial load, the Lüders front was approximately parallel to the material plane of maximum shear stress[4].

As for batch annealed sheets there have been ruptures in all samples during local sheet strain without any expansion of strain in the whole measured length of tested samples (see Fig. 3 and 4).

In Figs. 5 and 6, the surface failures of tested samples are shown. From Fig. 5a) we can expressly conclude that except primary slip planes where the rupture of tested samples appeared, also the so called secondary slip planes appeared in their proximity.

Local thinning of tested sheet has occurred in these places, as well. In the rest of measured part the tested sample has not been plastically deformed. The rupture surface in Fig. 5a, but also the detail in Fig. 5b and in Fig. 6 show, that in the place of sample rupture a sharp contraction (necking) has occurred. It points at the fact that the materi-

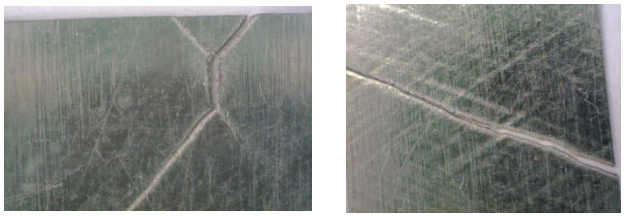

Fig. 3. **Rupture of samples after uniaxial tensile test of TH550CA (left) and TS550BA (right) with several slip planes**

Fig. 4. **Single slip plane of TH550CA tinplate (left) and multiple slip planes of TS550BA (right)**

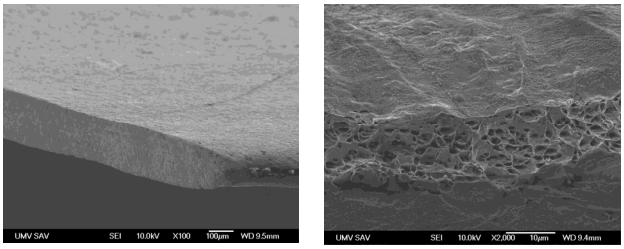

a b

Fig. 5. **Fracture of the TH550CA, a) side view, b) the detail of fracture surface**

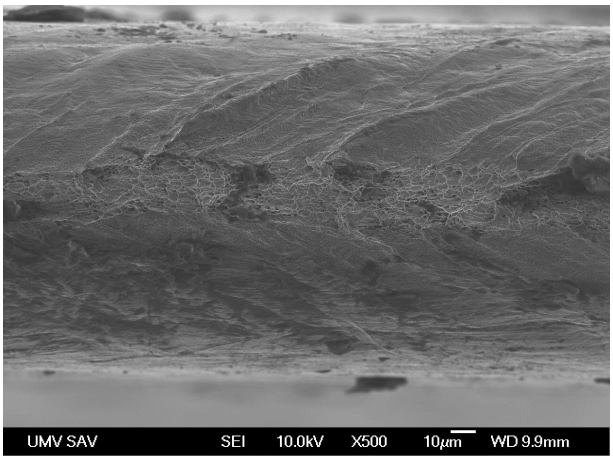

Fig. 6. **Perpendicular view of fracture surface and slip planes of TH550CA tinplate**

al itself has better plastic properties than the plastic properties measured by method of elongation at uniaxial tensile test.

3. Experimental results and discussion

Mean value of elongation of the sheets from 1 to 3 % was measured. Significant differences in mechanical properties were observed in the direction of 0° and 90°. In most cases, the difference of elongation was about 100 %. The results of mechanical tests showed that the uniaxial test of tinplates, especially double reduced, does not provide a true representation of their plastic properties. This fact is fully reflected in cupping test when the cups from packaging steel sheets with an elongation from 1 to 3 % were produced (LDR = 1.67) (ref.[7–9]). Despite very low values of the elongation, it was found that the failure is typical plastic (Fig. 7) and there is a large contraction (Fig. 5). From the details of fracture surface in Fig. 5b, but mainly from Fig. 6, we can clearly see the slip planes which are observed on the surface of the sheet near the fracture as waves. Thus, these tinplates have the local plasticity, but either the plastic strain is inhomogeneous on the whole gage section of the sample or plastic strain propagates only in local band and continue to failure. This cross-section is not able to transfer the strength necessary for the strain of another section of tested sample. The fracture surface shows characteristic signs of plastic intercrystalline fracture expanding along grain boundaries where inclusions can be found.

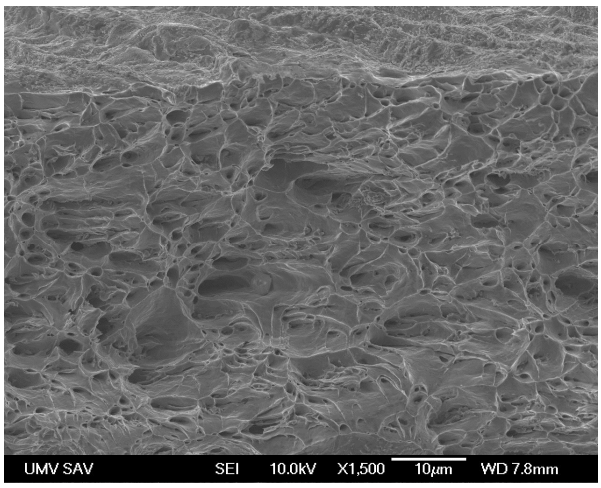

Fig. 7. **A detail view of fracture surface of TH550CA**

A general concept is that the end of the plateau is the starting point of homogeneous deformation in the gage section. However, the results shown that at the end of the plateau, the local deformation was still inhomogeneous. The inhomogeneous deformation persisted in the work-hardening stage. This observation is consistent with that observed by other researchers[4,6]. It was found that the local axial strain increased linearly and rapidly with time, indicating the propagation of the Lüders front over the area. A large amount of ferrite grains within this area experienced plastic deformation. For a mild steel, authors[7] pointed out that the strain rate at the Lüders front was rather high and some dislocations unable to move at the high strain rate can continue to move at a slow velocity after the front has passed them. Some deformed ferrite grains may deform further and some undeformed ferrite grains may experience a delayed plastic deformation. Such actions result in creep deformation. Similar phenomenon was observed in a monotonic tension of a mild steel[6] and an aluminum alloy[8].

Localization of deformation and fracture in a tensile test samples can be explained by the Marciniak theory,

whereby the localization of deformation occurs in areas with material inhomogeneity. Inhomogeneity can be represented by changing the microgeometry of the surface of the material or inhomogeneity (inclusions, cracks caused by one particular reduction of the grain boundaries). Failure of samples is probably initiated by the creation of the local neck in a certain place of the sample. This results in earlier failure and lower ductility. Thus, so narrow region cannot further transmit escalating loading and failure occurs just in this area.

4. Conclusions

In this paper, the causes and diversity of inhomogeneous strain were studied. The failure of tinplates during plastic deformation of simple uniaxial test sample was analysed. Experiments showed that plastic deformation of the samples during loading occurs only in certain places. This means that the plastic deformation do not extend to whole volume of the sample. On the other hand, the analysis of the fracture surface indicates that there is no brittle fracture. From achieved contraction of the sample it is clear that ductile fracture is concerned. This phenomenon can be attributed to inhomogeneity of the material structure, while the way of annealing of the material and structural inclusions, respectively, influence behaviour of the tinplates during loading. One of the conclusions is that there is usually either a one slip plane (TH550CA) with localization of the deformation in the slip plane up to failure or more slip planes (TS550BA) with Lüders bands. More slip planes may be related to the fact that microstructure of the TS550BA tinplate include a larger grains.

This contribution is the result of the projects implementation: Center for research of control of technical, environmental and human risks for permanent development of production and products in mechanical engineering (ITMS:26220120060) supported by the Research & Development Operational Programme funded by the ERDF and VEGA 1/0396/11.

REFERENCES

1. The European Standard EN 10202:2001, Cold Reduced Tin mill Products—Electrolytic Tinplate And Electrolytic chromium/Cr Oxide Coated Steel, The European Standard Publications, Brussels, 2001.
2. Pepelnjak T., Barisic B.: J. Mater. Proc. Technol. *186*, 111 (2007).
3. Barisic B., Pepelnjak T., Kuzman K.: J. Adv. Mater. Res. *6–8*, 329 (2005).
4. Zhang J., Jiang Y.: Int. J. Plasticity *21*, 651 (2005).
5. Yoshida F., Kaneda Y., Yamamoto S.: Int. J. Plasticity *24*, 1792 (2008).
6. Zhang J., Jiang Y.: ASME J. Eng. Mater. Tech. *126*, 164 (2004).
7. Kyriakides S., Miller J. E.: J. Appl. Mech. *67*, 645 (2000).
8. Onodera R., Nonomura M., Aramaki M.: J. Jpn. Inst. Metals *64*, 1162 (2000).
9. Spišák E., Majerníková J.: *Plastic deformation of tin coated steel sheet under different stress-strain states*. In: Progressive technologies and materials. 3-B: Materials, 2009. pp. 25–35.
10. Spišák E, Slota J., Majerníková J: Chem. Listy *105*, s485 (2011).
11. Hall E. O.: *Yield Point Phenomena in Metals and Alloys*. p. 36. Plenum Press, New York 1970.
12. Ananathan V. S., Hall E. O.: Scripta Metall. *23*, 1075 (1989).
13. Ananathan V. S., Hall E. O.: Acta Metall. Mater. *39*, 1353 (1991).
14. Lomer W. M.: J. Mech. Phys. Solids *1952*, 64.
15. Butler J. F.: J. Mech. Phys. Solids *10*, 313 (1962).
16. Morrison W. B., Glenn R. C.: J. Iron Steel Inst. *206*, 611 (1968).

E. Spišák, J. Slota, J. Majerníková, Ľ. Kaščák, and P. Malega *(Faculty of Mechanical Engineering, Technical University of Košice, Košice, Slovak Republic):*
Inhomogeneous Plastic Deformation of Tinplates under Uniaxial Stress State

Tinplates are mainly processed by forming nowadays. It is necessary to know their properties for the evaluation of their suitability for the forming processes. The paper deals with the inhomogeneous plastic deformation during uniaxial loading and the localization of plastic deformation which lead to the early failures of the tinplates. Causes of inhomogeneous strain and local propagation of deformation were analyzed.

JOINING MATERIALS USED IN CAR BODY PRODUCTION BY CLINCHING

EMIL SPIŠÁK[a] , ĽUBOŠ KAŠČÁK[a], and JACEK MUCHA[b]

[a] *Technical University of Košice, Faculty of Mechanical Engineering, Department of Technology and Materials, Mäsiarska 74, 040 01 Košice, Slovakia,* [b] *Rzeszow University of Technology, ul. Wincentego Pola 2, 35-959 Rzeszów, Poland*
lubos.kascak@tuke.sk

Keywords: clinching, car body sheets, evaluation of properties

1. Introduction

The automotive industry is currently working to accommodate the conflicting requirements of both environmental legislation and customer demands for greater performance and more luxury and safety features, by developing a light-weight and therefore essentially, energy-efficient vehicle[1]. One of the possibilities of decreasing the car weight and consequently lowering the fuel consumption is using various combinations of materials, such as combination of conventional deep-drawn steel sheet and high-strength steel sheet. In the areas, where high passive safety is needed, high-strength steels such as TRIP can be used. The usage of such steels can significantly reduce the car weight[2].

The increasing use of coated, lightweight and high-strength materials has led the automotive industry to re-examine traditional methods of component assembly. For example, direct welding of dissimilar sheet metals has proven to be difficult or impossible; thus, alternative joining techniques, such as mechanical fastening systems, have attracted increasing interest and applications in recent years. Mechanical fastening encompasess a broad range of methods, from threaded fasteners to different forms of rivets and mechanical interlocking methods[3].

One of these methods is clinching technology, which has not attracted much attention from researchers as yet, so it has not been studied deliberately so far. Clinching does not use any kind of appending joining components (such as screws, bolts)[4].

Only a die and a punch are used to press the sheet components to finish the whole joining process. The clinching process is a combination of drawing and forming that locks together sheets metal layers. The blanks are plastically deformed and the shape of the tools remains theoretically unchanged during the clinching processes. The punch is movable, whereas the fixture and the die are fixed during the process. The punch force needed for the joining process depends on the thickness and the strength of the materials to be joined, the size of the tools and friction coefficient usually varies from 10 to 100 kN (ref.[5,6]).

The paper evaluates joints made by clinching the following materials: microalloyed steel HSLA H220PD, TRIP steel 40/70+Z100MBO and drawing grade steel DX51D+Z.

Table I
Basic mechanical properties of used materials (*not specified)

	$Rp_{0.2}$ [MPa]	Rm [MPa]	A_{80} [%]	n_{90}
H220PD	238	382	36	0.228
TRIP40/70	450	766	26	0.278
DX51D+Z	≥ 140	270-500	≥ 22	*

2. Materials and methods

The following steel sheets were used for experimets: microalloyed steel HSLA H220PD with the thickness of

Table II
Chemical composition (wt.%) of used materials

Material	Chemical composition in [%] wt.									
	C	Mn	Si	P	S	Al	Cu	Ni	Cr	Ti
H220PD	0.06	0.7	0.5	0.080	0.025	0.020	0.011	0.017	0.310	0.037
TRIP 40/70	0.204	1.683	0.198	0.018	0.003	1.731	0.028	0.018	0.055	0.009
DX51D	0.64	0.178	0.007	0.016	0.002	0.120	0.041	0.02	0.023	0.002
	V	Nb	Mo	Zr						
H220PD	0.002	0.026	0.005	0.001						
TRIP 40/70	0.004	0.004	0.008	0.007						

0.8 mm, TRIP 40/70+Z100MBO with the thickness of 0.77 mm and DX51D+Z with the thickness of 0.9 mm.

Their basic mechanical properties and chemical composition are shown in Tables I and II. Mechanical properties of DX51D steel were specified by producer.

According to the orientation of punch and die to the position of upper and lower joined material, following combinations of steel sheets for press joining were used:

- *Samples A*:
H220PD (a_0 = 0.80 mm) and TRIP (a_0 = 0.77 mm)*
- *Samples B*:
TRIP (a_0 = 0.77 mm) and H220PD (a_0 = 0.80 mm)*
- *Samples C*:
H220PD (a_0 = 0.80 mm) and H220PD (a_0 = 0.80 mm)
- *Samples D*:
TRIP (a_0 = 0.77 mm) and DX51D (a_0 = 0.90 mm)*
- *Samples E*:
DX51D (a_0 = 0.90 mm) and TRIP (a_0 = 0.77 mm)*
(*sheet on the die side of press joining tool)

The samples with dimensions of 40 × 90 mm and 30 mm lapping according to STN 05 1122 standard were used for the experiments (Fig. 1). Six samples were prepared for every combination of sheets. It is not necessary to clean the surfaces of samples before clinching[7].

Clinching was performed on the tension machine ZD 40 made by Werkstoffprüfmaschinen Leipzig Company with the loading range of 40 kN. The force needed for joining was 30 kN. The carrying capacities of the clinched joints were evaluated according to standard STN 05 1122 – Tensile test of spot welded joints. This test was used for measuring the maximum carrying capacities Fmax of the clinched joints. The test was carried out on the metal strength testing machine TIRAtest 2300 produced by VEB TIW Rauenstein, with the loading speed of 8 mm min^{-1}.

Further tests for quality evaluation of clinched joints included the metallographical analysis and microhardnesses analysis according to STN EN ISO 6507-1 standard. Microhardness analysis was performed on the sample C with HSLA H220PD sheets.

The results of carrying capacities of clinched joints were compared with the carrying capacities of resistance spot welded joints.

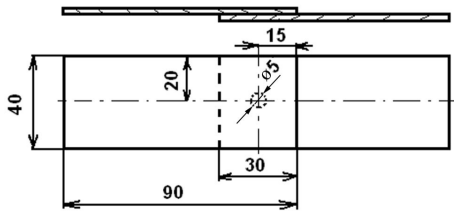

Fig. 1. **Dimensions of samples for the tensile test and principle of clinching**

3. Results

The measured values of carrying capacities of clinched joints after tensile test in comparison with the measured values of carrying capacities of resistance spot welded joints are shown in Table III. The resistance spot welded joints were made with the optimized values of welding parameters[2,8]. The resistance spot welds of all observed samples reached higher values of carrying capacities in comparison with clinched joints. On average, the clinched joints reached 13 % (samples A), 18 % (samples C) and 21 % (samples E) of carrying capacities of resistance spot welds.

The carrying capacities of samples B and samples D were not measured, because the joints were not successfully made. The upper sheets of both samples (TRIP 40/70 steel) were cut off in the place of the joint and then pressed to the lower sheet (Fig. 2).

The average value of carrying capacities of samples A was 1008 N. The cracks in the TRIP steel were observed on the die side (Fig. 3), which could possibly have a negative effect, especially during dynamic load. The cracks can even decrease the joints' corrosion resistance. The values

Table III
Measured values of carrying capacities

Number of sample	Carrying capacity Fmax [N]					
	Samples A		Samples C		Samples E	
	CJ	RSW	CJ	RSW	CJ	RSW
1	939	7310	980	5305	1087	7420
2	985	7641	1008	5290	1584	7644
3	1016	7680	956	5072	1334	7710
4	1080	7172	924	5260	1834	7417
5	1093	7417	973	5238	1973	7565
6	937	7581	978	5177	1658	7513

CJ – clinched joints, RSW – resistance spot welded joints

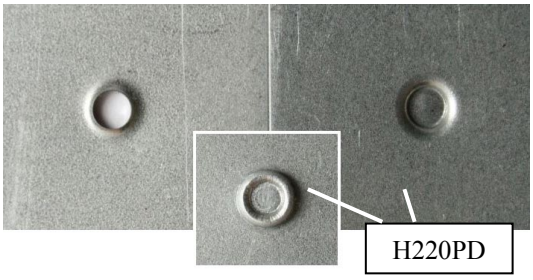

Fig. 2. **Sample B without creating a clinched joint**

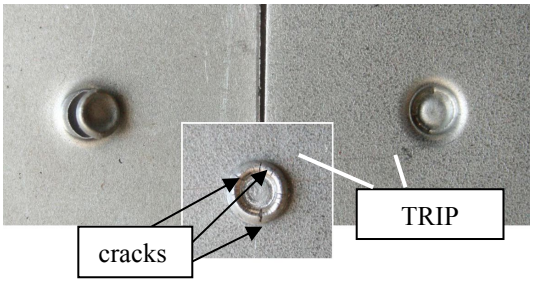

Fig. 3. **Sample A after tensile test with cracks in the CJ joint**

of carrying capacity of samples A are similar to the values measured in clinched joints of the common drawing grade steel sheets, as was published in[6].

The average value of carrying capacity of samples C was 970 N. No cracks occurred in the place of the joint from the side of the die. The carrying capacity values of samples C are similar to the values measured in clinched joints of common drawing grade steel sheets.

The average value of carrying capacity of samples E was 1578 N. Cracks in the TRIP steel on the die side were observed, similar to those in sample A (Fig. 3). The measured values of carrying capacity of samples E are higher than those of samples A and C, which is probably caused by the thicker material of the upper sheet in the joint (DX51D of 0.9 mm).

Figs. 4 and 5 shows the obtained load–displacement curves of clinched joints and spot welded joints os the sample C. The maximum load value of clinched joint is about 1000 N and the maximum load value of spot welded joint is about 5000 N. Fig. 6 shows the obtained load–displacement curves of clinched joints of all successfully made samples A, C, and E. The curve shapes of samples A and C are very similar as well as the values of their carrying capacities.

The metallographical analysis confirmed that the area with the most significant thinning in the joint is its critical area (Fig. 7).

There occured failures in such areas during tensile tests of samples A, C and E, and during the clinching process in samples B and D. The metallographical analysis confirmed the occurrence of cracks in the TRIP steel on the die side of the joints in the round part (Fig. 8).

Fig. 9 presents a sample C with marked areas of microhardness measurements and the measured values. The

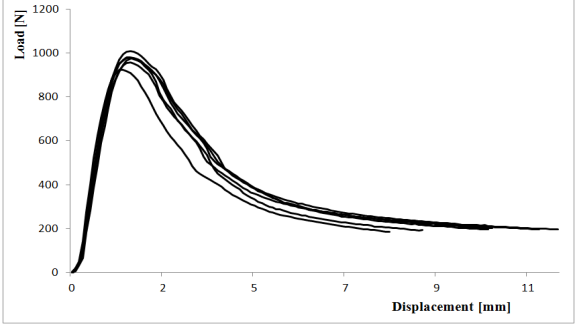

Fig. 4. **Load–displacement curves of clinched joints – sample C**

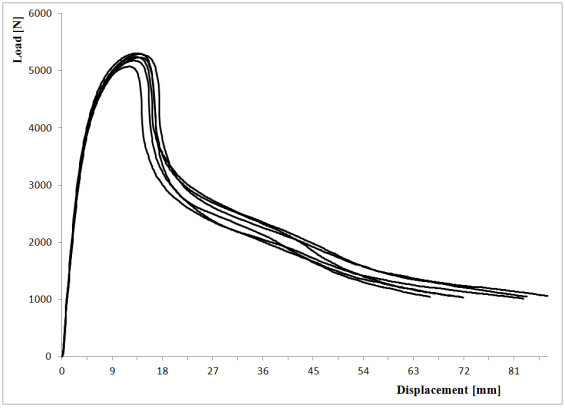

Fig. 5. **Load–displacement curves of spot welded joints–sample C**

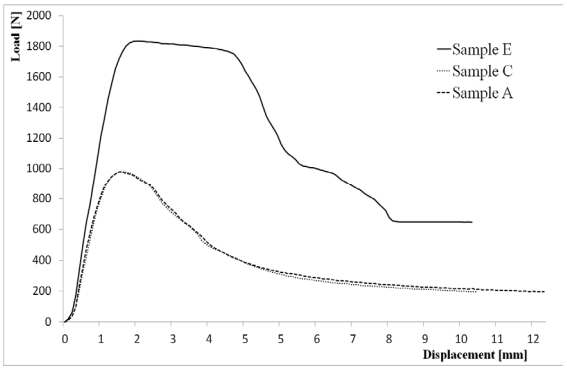

Fig. 6. **Load–displacement curves of clinched joints**

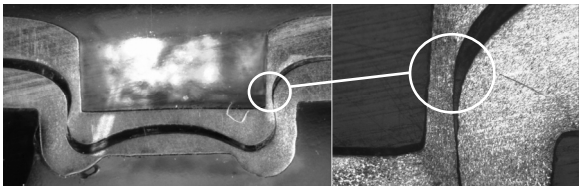

Fig. 7. **The critical area of clinched joint – sample C**

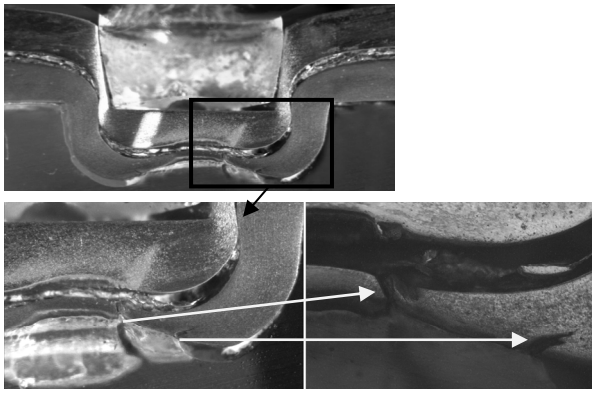

Fig. 8. **The cracks in TRIP steel on the side of die – sample A**

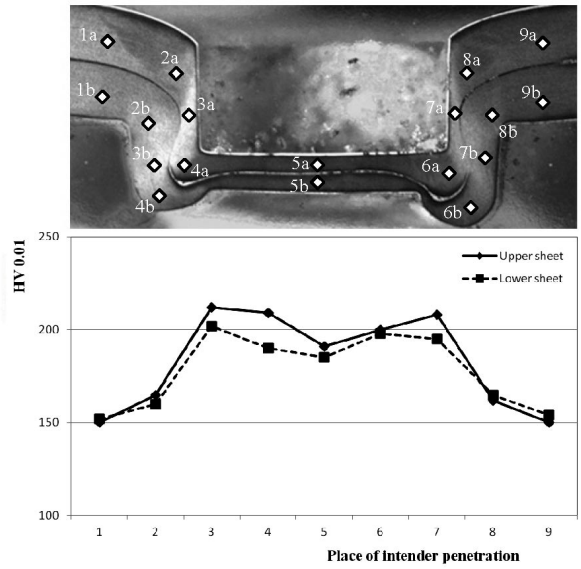

Fig. 9. **Microhardness values of the sample C**

measurements show the changes in the clinched joint, where the highest microhardness vaules were measured in the critical area of the clinched joint.

4. Conclusion

The paper focused on the evaluation of clinched joints of various material combinations. Microalloyed steel HSLA H220PD, TRIP steel 40/70+Z100 MBO and DX51D+Z steel were used for the experiments.

The influence of the orientation of joined materials regarding the position of punch and die of the tool was also observed. The material combinations of TRIP 40/70 with H220PD as well as TRIP 40/70 with DX51D, where TRIP steel is oriented towards the punch, are not suitable for joining by clinching, because the joints were not successfully created. Failures occur during the clinching process in the critical areas of joints. The same material combinations where TRIP steel is oriented towards the die proved to be unsuitable for joining by clinching, even though joints were created, because there occur cracks in TRIP steel, which could negatively affect the joint, especially during dynamic load. The cracks can even decrease the corrosion resistance of the joints.

The only combination that proved to be suitable for joining by clinching was a combination of H220PD materials – sample C. The carrying capacities of these samples were sufficient and the metallographical analysis confirmed no occurrence of cracks or failures in the area of clinched joints. The carrying capacity of these joints reached about 20 % of the carrying capacity of resitance spot welded joints of the same materials.

The paper was elaborated within the project Center for research of control of technical, environmental and human risks for permanent development of production and products in mechanical engineering (ITMS:26220120060).

REFERENCES

1. Barnes T. A., Pashby I. R.: J. Mater. Proc. Technol. *99*, 72 (2000).
2. Spišák E., Kaščák Ľ., Viňáš J.: Chem. Listy *105*, s448 (2011).
3. Sun X., Khaleel M. A.: J. Man. Processes *7*, 83 (2005).
4. Nong N., Keju O., Yu Z., Zhiyuan Q., Changcheng T., Feipeg L.: J. Mater. Proc. Technol. *137*, 159 (2003).
5. Varis J. P.: J. Mater. Proc. Technol. *174*, 275 (2006).
6. Kaščák Ľ., Spišák E.: Scient. Bulletins of Rzeszów University of Technology: Mechanics *73*, 161, (2008).
7. Mucha J., Kaščák Ľ., Spišák E.: Arch. Automot. Eng. *3*, 185 (2010).
8. Kaščák Ľ., Spišák E., Mucha J.: Scient. Bulletins of Rzeszów University of Technology: Mechanics *80*, 121, (2010).

E. Spišák[a], Ľ. Kaščák[a], and J. Mucha[b] *([a] Technical University of Košice, Faculty of Mechanical Engineering, Department of Technology and Materials, [b] Rzeszow University of Technology, Rzeszów, Poland):* **Joining Materials Used in Car Body Production by Clinching**

The paper dealt with the evaluation of properties of joints made by clinching. The microalloyed steel H220PD (a_0 = 0.8 mm), the high strength steel TRIP 40/70+Z100MBO (a_0 = 0.77 mm) and the drawing grade steel DX51D+Z (a_0 = 0.9 mm) were used for the experiments. The orientation of joined materials regarding the position of punch and die of the tool has the significant effect to carrying capacities of the joints. The TRIP steel steel is not suitable material for press joining method, even with both observed combination – with H220PD or DX51D. The carrying capacity of these joints was approximately 20 % of the carrying capacity of resitance spot welded joints.

NANOINDENTATION TESTING OF COMPOSITE BASED ON COLLAGEN AND POLY(DL-LACTIDE) NANOFIBERS

TOMÁŠ SUCHÝ[a,b], ZBYNĚK SUCHARDA[b], MONIKA ŠUPOVÁ[b], KAREL BALÍK[b], JOSEF ŠEPITKA[a], and JAROSLAV LUKEŠ[a]

[a] Czech Technical University in Prague, Fac. of Mechanical Eng., Dept. of Mechanics, Biomechanics and Mechatronics, Laboratory of Biomechanics, Technická 4, 166 07 Prague 6, [b] Institute of Rock Structure and Mechanics, ASCR, v.v.i., Dept. of Composite and Carbon Materials, V Holešovičkách 41, 182 09 Prague 8, Czech Republic tomas.suchy@fs.cvut.cz

Keywords: nanoindentation, poly(DL-lactide), collagen, composite, nanofibers

1. Introduction

In bone tissue engineering, there is a great need to engineer multi-phase materials that combine the advantages exhibited by each component of the material, and that have a structure and composition similar to that of natural bone[1]. In our project, we design biomimetic nanocomposite materials that promote the regeneration of defective bone tissue with the required rate of biodegradation. The proposed composition of the material imitates the real bone structure, and combines the advantages of nano fibers, aliphatic polyesters, collagen, and calcium phosphates. This study uses nanoindentation to evaluate the influence of various weight fractions of polymeric nanofibrous phase on the mechanical properties of a composite based on collagen type I matrix and poly(DL-lactide) nanofibers (PDLL). The preparation of composite test samples for nanoindentation and the structure of the samples are discussed.

2. Materials and methods

Composites based on PDLL (PURASORB PDL 05, Purac Biomaterials, the Netherlands; inherent viscosity 0.5 dl g^{-1}) nano fibers and collagen type I matrix were prepared. A poly(DL-lactide) nanofibrous omnidirectional filler (Fig. 1) was prepared by electrospinning (NS 8A 1600, Elmacro Ltd., Czech Republic) from a chloroform solution[2]. Collagen matrix ISC_{40} was isolated from fish skin (carp) under denaturing conditions (40 °C, acetic acid, 30 min) followed by lyophilization according to Pešáková et al.[3] Composite samples were prepared with 6 different weight fractions of nanofibers (0, 60, 70, 73, 80, 87 wt.%) and hardened onto polymethylmethacrylate supporting plates (AZ Plastik, Czech Republic).

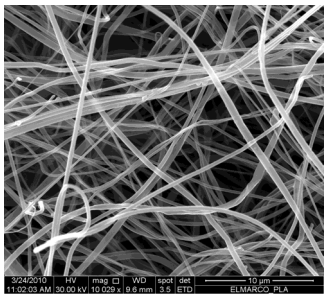

Fig. 1. **SEM micrograph of poly(DL-lactide) omnidirectional nanofibers (mag. x 10,000)**

Briefly, all composite samples were prepared by impregnation of PDLL with collagen/deionized water dispersion. The collagenous dispersion was prepared in the IKA DI18 homogenisator (IKA Werke GmbH, Germany) (at a rotation speed of 20.000 min^{-1} for 2 minutes) by dispersion of 0.5 g of collagen in 100 g of deionized water. The weighed amount of the PDLL nanofibrous layer was placed on to separating foil and impregnated with a weighed amount of collagenous dispersion in order to achieve the chosen weight fraction of the nanofibrous filler after water evaporation (at room temperature). Four layers prepared using this procedure were cut into an appropriate size and laid on a polymethylmethacrylate supporting plate. Finally, the supporting plate and the composite were covered by a separating foil and hardened at 50 °C under a pressure of 4 kPa. A relatively low temperature was chosen to be below the glass-transition temperature of collagen[4] and PDLL[5].

The assessment of various weight fractions of the nanofibrous phase on the mechanical properties (reduced elastic modulus E_r) of the composites was studied using the nanoindentaion mode, which is an option of the Hysitron TriboIndenter™ TI 950 nanomechanical instrument (Hysitron, USA). A Berkovich diamond fluid tip with apex radius ~120 nm was used for the nanoindentation tests. For each tested composite, indents were applied on five 60 × 60 μm areas as a matrix of 5 × 5 indents with 15 μm separation (with 25 μN applied force, lift height 100nm, preload 1 μN).

The prepared composites were also investigated by image analysis, using a QUANTA 450 electron SEM microscope (FEI Company, USA) under a high vacuum, with an Au coating film on the samples.

A statistical evaluation was carried out using the following methods (STATGRAPHICS Centurion XV, StatPoint, USA): the statistically significant differences were checked by nonparametric methods (the Kruskal-

Wallis test, $\alpha = 0.05$); the Mann-Whitney test was used as a post hoc test ($\alpha = 0.05$); and the confidence intervals for the mean values were calculated at a significance level of $\alpha = 0.05$.

3. Results and discussion

The reduced elastic modulus of composites based on collagen matrix and PDLL a nanofibrous phase was measured (Fig. 2).

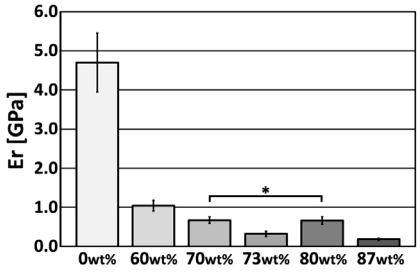

Fig. 2. **The reduced modulus E_r of the tested composites** (* denotes values without statistically significant differences, Mann-Whitney post hoc test, $\alpha = 0.05$)

The obtained value for the modulus of pure collagen matrix (0 wt.%) is in reasonable agreement with earlier results obtained by various methods (2–11.5 GPa)[6,7]. After additions of 60 wt.% of nanofibers, the modulus decreases markedly from 5.45–3.95 GPa to 1.17–0.91 GPa. A further decrease in the reduced modulus (in the case of composites with 70–87 wt.% of PDLL) is less marked.

It can be deduced from the trend of this decrease that the higher the amount of PDLL, the lower the reduced modulus will be. This finding can be explained by the lower elastic modulus of the PDLL precursor used for electrospinning the nanofibers (0.47–0.59 GPa)[2]. The omnidirectional orientation of the nanofibrous phase and mainly the porosity of the composites are probably other important factors that influence the process (Fig. 3). It should be noted that the E_r values can also be partly attributed to the fact that in nanoindentation the Young's modulus represents the lateral elasticity at the surface, rather than the bulk stiffness. For further analyses in our study, it will be necessary to improve the preparation of the composite samples. The improvement will focus on a superior fibrous phase filling with collagenous matrix, and on applying the hardening process under higher pressure. The porosity of the samples will be analysed.

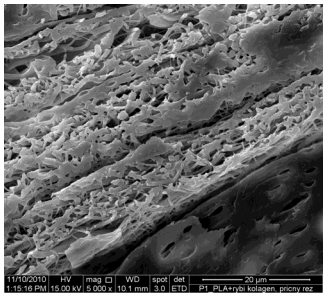

Fig. 3. **SEM micrograph of a cross section of the collagen/ PDLL (60 wt.%) composite illustrates the apparent porosity (mag. x 5 000)**

4. Conclusion

The results provide an assessment of the different weight fraction of the composite reinforcing phase. In general, the PDLL nanofibrous phase decreases the elastic modulus of the composites studied here. The nanoindentation method seems to be a suitable tool for determining the mechanical properties of composite materials variously modified at the nanoscale.

This research was supported by the Czech Science Foundation (project No. 106/09/1000), and by Ministry of Education project Transdisciplinary Research in Biomedical Engineering II., No. MSM 6840770012.

REFERENCES

1. Cancedda R., Giannoni P., Mastrogiacomo M.: Biomaterials *28*, 4240 (2007).
2. Gao Y., Kong L., Zhang L., Gong Y., Chen G., Zhao N., Zhang X.: Eur. Polym. J. *42*, 764 (2006).
3. Pešáková V., Štol M., Gillery P., Maquart F. X., Borel J. P., Adam M.: Biomed. Pharmacother. *48*, 261 (1994).
4. Yan M., Li B., Zhao X., Ren G., Zhuang Y., Hou H., Chen L., Fan Y.: Food Chem. *107*, 1581 (2008).
5. Garlotta D.: J. Polym. Environ. *9*, 63 (2001).
6. Wenger M. P. E., Bozec L., Horton M. A., Mesquida P.: Biophys. J. *93*, 1256 (2007).
7. Meyers M. A., Chen P. Y., Lin A. Y., Seki Y.: Prog. Mater. Sci. *53*, 1 (2008).

T. Suchý[a,b], Z. Sucharda[b], M. Šupová[b], K. Balík[b], J. Šepitka[a], and J. Lukeš[a] *([a] CTU in Prague, Fac. of Mechanical Eng., [b] Institute of Rock Structure and Mechanics, ASCR, v.v.i., Czech Republic):* **Nanoindentation Testing of Composite Based on Collagen and Poly(DL-Lactide) Nanofibers**

The influence of various weight fractions (0, 60, 70, 73, 80 and 87 wt.%) of the poly(DL-lactide) nanofibers on the mechanical properties of the composite based on collagen type I matrix was evaluated by nanoindentation. After addition of 60 wt.% of nanofibers, the reduced elastic modulus decreases markedly (from 5.45–3.95 GPa to 1.17–0.91 GPa) while a further decrease (70–87 wt.%) is less marked.

MICROMECHANICAL PROPERTIES OF DIFFERENT MATERIALS ON GYPSUM BASIS

PAVEL TESÁREK, TOMÁŠ PLACHÝ, PAVLA RYPAROVÁ, and JIŘÍ NĚMEČEK

Czech Technical University in Prague, Thákurova 7, 166 29 Prague, Czech Republic
pavel.tesarek@fsv.cvut.cz

Keywords: nanoindentation, gypsum, micromechanical properties, deconvolution, homogenization

1. Introduction

Gypsum hydration starts right after the mixing of water with gypsum. The process of hydration and setting depends on multiple factors[1]. These effects can be observed on several scales. Usually, two levels (micro- and macro-scale) are considered at least. Material properties of hardened gypsum on macro-level (e.g. thermal and mechanical properties) depend on the material structure (namely porosity) and prevailing matrix properties[2]. As the main factor, water to gypsum ratio determines the value of total porosity which is an effect of over-stoichiometric water. Micro-level material properties depend on microstructural parameters like chemical purity of the used gypsum (plaster); ratio between the three main components of the gypsum binder, i.e. calcium sulfate anhydrite (different phases), calcium sulfate hemihydrate α- or β-gypsum and calcium sulfate dihydrate[3,4]; some impurities and eventually additives; size and ordering of calcium sulfate dihydrate crystals[1,5], etc.

The main objective of this paper was to compare macro- and micro-elastic properties of studied gypsum materials and to find the dependence between macro- and micromechanical properties in connection with porosity.

2. Materials and samples

Three different materials on gypsum basis were selected for the testing. The first one was commercially available dental gypsum Interdent® based on α-calcium sulfate hemihydrate ("Dental gypsum series"). The water to gypsum ratio was 0.2 in this case[6]. The second one was a flue gas desulphurization gypsum (FGD) based on β-calcium sulfate hemihydrate produced at Electric Power Station Počerady (Czech Republic). These samples were denoted as "FGD gypsum series". The water to gypsum ratio was 0.627 in this case. The last series was commercially produced grey gypsum based on β-calcium sulfate hemihydrate (Gypstrend Ltd. – Kobeřice near Opava in Czech Republic) denoted as grey gypsum (after typical color of this gypsum which contained 50 % of natural calcium sulfate dihydrate). The water to gypsum ratio was 0.71. Table I shows the basic material properties as bulk density, total porosity and values of micro-porosity lower then 1 μm. This part of the porosity was assumed to be naturally included in the nanoindentation data since the indentation volume under the tip covered a region of ~1–2 μm^3.

Table I
Basic material properties of the tested samples

Material	Bulk density [kg m^{-3}]	Total open porosity [m^3 m^{-3}]	Open porosity lower then 1 μm [m^3 m^{-3}]
Dental gypsum	2020	0.19	0.12
FGD gypsum	1220	0.51	0.14
Grey gypsum	980	0.61	0.13

3. Experimental methods and results

First, the macroscopic values of dynamic Young's modulus on macro-level were measured by non-destructive impulse excitation method[7] which is based on measuring the fundamental resonant frequencies. The test arrangement was done for longitudinal vibration. The specimen with dimensions of 40×40×160 mm was supported in the midspan, i.e. the fundamental longitudinal nodal position. The acceleration transducer Bruel&Kjaer of Type 4513B was placed at the centre of one sample end face. The opposite end face was hit by the impact hammer Bruel&Kjaer, Type 8206. From the obtained results, the weight of the sample and the dimension of the sample, values of dynamic Young's modulus were calculated[7]. Total open porosity and values of micro-porosity were calculated from results obtained from mercury porosimetry and pycnometric density measurements.

Micromechanical properties of dental gypsum samples were measured by using CSM Nanohardness tester. Quasi-static loading consisted of 10 s of linear loading (rate 30 mN min^{-1}), 10 s of holding period at constant peak force 5 mN and 10 s of unloading (rate 30 mN min^{-1}). The distance between individual indents was set 15 μm to avoid mutual influences[9]. Elastic constants were evaluated for individual indents by standard Oliver and Pharr methodology[8]. Poisson's ratio was estimated to be 0.2 for all cases. Grid nanoindentation and deconvolution techniques were applied[9]. Three phase microstructural system was assumed based on the shape of experimental histograms of elastic moduli[6]. Thus, the anisotropy of gypsum

crystals was replaced by the phase differences at a deconvolution process[6,9]. The dental gypsum composed of one dominant phase (E=37.2 GPa, 71.2 %) and two minor phases (E=19.4 GPa, 4.4 % and E=56.3 GPa, 24.4 %) [6,10].

To compare results from different methods, macroscopic elastic properties were predicted from analytical homogenization scheme, namely Mori-Tanaka method[10], with the assumption of a two-phase composite – matrix (having the properties received from nanoindentation and lower level homogenization[9,10] of the three phase system and air pores larger than 1 μm. The homogenized Young's modulus for the matrix was 34.8 GPa. Results from macroscopic dynamic measurements showed on the value 36 GPa, i.e. the agreement of the macroscopic value and the micromechanically predicted one was within 3.3 % in this case.

Since the direct micromechanical measurements on FGD and grey gypsum samples faced significant obstacles in the form of very high porosity and roughness it was decided to use inverse analysis and predict micromechanical properties of the matrix from the macroscopic ones using the same principles as in case of dental gypsum. The obtained results are summarized in Table II. It can be seen that micro elastic properties of FGD and grey gypsum samples (based on β-gypsum composition) are approximately 2.6–2.8× lower then those for dental gypsum (α-gypsum composition).

Table II
Measured/calculated Young's moduli

Gypsum	Macroscopic Young's modulus [GPa]		Microscopic (homogenized matrix) Young's modulus [GPa]
Dental	36/34.8	←	40.0
FGD	7/-	→	15.2*
Grey	5/-	→	14.2*

Note: *denotes results obtained from inverse analysis. An arrow indicates the analysis direction

4. Conclusions

The paper presents comparison of micro- and macromechanical properties of several types of gypsum materials in dependence on their different chemical origin and porosity. Grid nanoindentation, statistical deconvolution and porosimetry were utilized. Good agreement within 3.3 % was found in case of dental gypsum samples based on α-gypsum composition. The analytical homogenization was used in the prediction of either microscopic matrix properties (for dental gypsum) or for the inverse analysis of microscopic properties from the known macroscopic ones (for FGD and grey gypsum samples). This analysis points on the approximately 2.6–2.8× lower microscopic elastic properties of β-gypsum based samples. Such hypothesis will be subsequently verified using nanoindentation which was beyond the scope of this contribution at present.

Support of the Czech Science Foundation (P105/12/0824) and Ministry of Education of the Czech Republic (MSM 6840770003) is gratefully acknowledged.

REFERENCES

1. Šatava V.: Ceramics–Silikáty *40*, 2 (1996).
2. Singh M.: Constr. Build. Mater. *19* (2005).
3. Garg M., Jain N., Singh M.: Constr. Build. Mater. *23* (2009).
4. Tydlitát V., Tesárek P., Černý R.: J. Therm. Anal. Calorim. 91, *3* (2008).
5. Arslan A. T., Koca M., Aydogmus Y. T., Klapperich H., Yılmaz H. R.: Rock Mech. Rock Engng. *41* (2008).
6. Tesárek P., Němeček J.: Chem. Listy *105*, s17 (2011).
7. Plachý T., Tesárek P., Wilczynska A., Padevět P.: *3rd WSEAS International Conference on Engineering Mechanics, Structures, Engineering Geology/ International Conference on Geography and Geology Location* (2010).
8. Oliver W., Pharr G.: J. Mater. Res. *7* (1992).
9. Němeček J., Šmilauer V., Kopecký L.: Cem. Concr. Compos. *33* (2) (2011).
10. Němeček J., Králík V., Vondřejc J., Němečková J.: *49th International Scientific Conference Experimental stress Analysis* (2011).

P. Tesárek, T. Plachý, P. Ryparová, and J. Němeček *(Czech Technical University in Prague, Faculty of Civil Engineering):* **Micromechanical Properties of Different Materials on Gypsum Basis**

Micro- and macro-level elastic properties of three types of gypsum samples (dental gypsum, flue gas desulphurization gypsum and grey gypsum) were compared. Grid nanoindentation, statistical deconvolution and porosimetry were used on lower composite level and non-destructive impulse method on macro-scale. The transition between the scales was computationally maintained by the Mori-Tanaka homogenization method. Good agreement was achieved between experiments and numerical prediction.

Obtained results also showed that the micro-elastic properties predicted (by inverse analysis) for FGD and grey gypsum samples (β-gypsum composition) are approximately 2.6–2.8× lower then those for dental gypsum (α-gypsum composition).

IMPACT OF BLEACHING GELS ON DENTAL ENAMEL MICROHARDNESS AND 3D SURFACE ROUGHNESS

QUANG DUNG TRAN[a], KAREL MAŇAS[a], EMIL SVOBODA[a], MICHAL BUMBÁLEK [b], and ZDENĚK JOSKA[a]

[a] *Department of Mechanical Engineering, University of Defence in Brno, Kounicova 65, 612 00 Brno,* [b] *Department of Dental Care, Faculty of Medicine, Masaryk University, Kamenice 753/5, 625 00 Brno, Czech Republic*
dungchm@yahoo.com

Keywords: enamel, bleaching, microhardness, 3D surface roughness

1. Introduction

At this time, the popularity of dental bleaching has increased in esthetic dentistry. Tooth bleaching using different oxidizing agents as hydrogen peroxide or carbamide peroxide is one of the most spread procedures[1–4]. The effect of bleaching treatment on dental enamel has long been a concern of many dentists, because bleaching agents react with enamel and cause chemical, structural and mechanical changes on the enamel surfaces. One of the most common methods of evaluation of changes in surface topography[5,6] is electron microscopy, stylus profilometery or atomic force microscopy[7]. The aim of this work is to investigate the effect of two different tooth bleaching gels containing 22 % carbamide peroxide and 38 % hydrogen peroxide on surface microhardness and properties of dental enamel by the 3D surface topography.

2. Materials and experimental methods

Four extracted teeth human third molars were used for experiment. Enamel slabs of 5.0×5.0×1.5 mm were cut from the buccal and lingual surfaces by using a precision slow speed diamond saw with water cooling. Each cut slab was embedded in dentacryl. Enamel surface was wet grounded to achieve flat surface by using 400, 600, 1000 and 2500 grit silicon carbide papers. Then the prepared slabs were placed in an ultrasonic cleaner for 3 min. Samples were stored in distilled water at room temperature prior to the experiment. A total of 8 enamel specimens were prepared for the experiments.

Two different bleaching gels were applied on the prepared specimens. For experiments, „in home“ Yotuel® Patient with 22 % carbamide peroxide (Biocosmetics Laboratories) and „in office“ Opalescence Boost with 38 % hydrogen peroxide (Ultradent products) were used. Yotuel® Patient was applied in 1 cycle for 3 hours and Opalescence Boost was applied in 4 cycles for 15 minutes. After bleaching treatment samples were cleaned in distilled water and Baseline microhardness was measured before treatment with a microhardness Vickers indenter (LECO LM 247 AT) at a 100 g load and 12 s dwell time. The mean Vickers hardness numbers (VHN) were derived from five indentations made across the enamel surface of each specimen.

After microhardness testing, surface topography of the specimens was evaluated on a 3D surface area by the Talysurf CLI 1000 device with non contact confocal gauge. The topography data were visualized and evaluated using commercial software Talymap Platinum. Measured area was 1.25×1.25 mm. The filter cut off which separates the roughness and waviness area λ_c was set to 0.25× 0.25 mm. These roughness parameters were measured: the core roughness depth S_k – the height difference between intersection points of the found least mean square line, the reduced summit height S_{pk} – the height of the upper left triangle and the reduced valley depth S_{vk} – the height of the triangle drawn at 100 %.

3. Results

The confocal microscopy image shows the bleached surface in Fig. 1. The measured values of microhardness of showed enamel before and after treatment remain almost the same (see Fig. 2).

The area measured by the Talysurf CLI 1000 device is shown in Fig. 3. The values of selected parameters before and after bleaching treatment are shown in Tab. I. The results show that bleaching gel Yotuel® Patient has a bigger impact on surface roughness parameters than Opalescence Boost PF. The results from amplitude distribution and material ratio curves (Fig. 4) confirmed that bleaching gels have effects on topography of enamel. After treat-

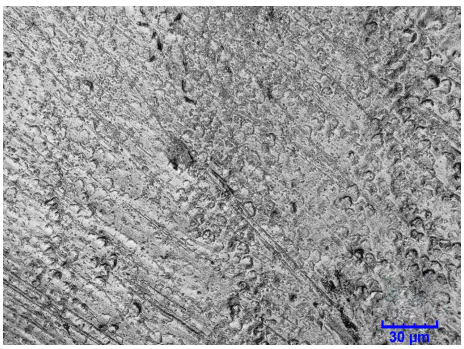

Fig. 1. **The bleached surface of dental enamel in a confocal micrograph**

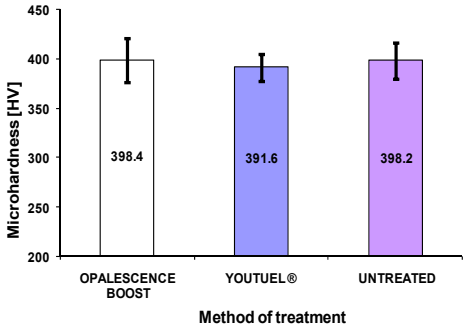

Fig. 2. **Enamel microhardness before and after treatment**

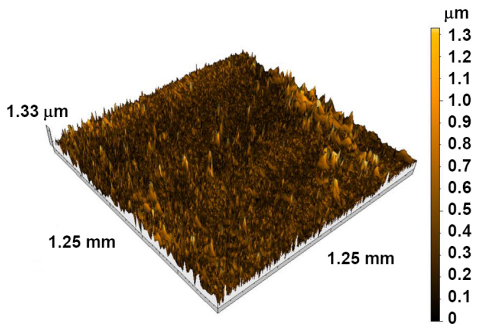

Fig. 3. **The 3D surface roughness of bleached enamel (Opalescence Boost)**

Table I
Values of (3D) surface roughness parameters

[µm]	Yotuel® Patient		Opalescence Boost PF	
	Grounded	Bleached	Grounded	Bleached
S_{pk}	0.416	0.626	0.416	0.565
S_k	0.426	0.213	0.470	0.453
S_{vk}	0.137	0.254	0.165	0.170

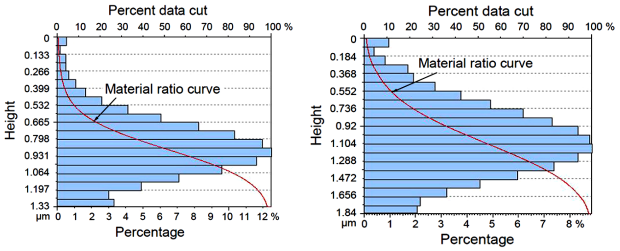

a) Opalescence Boost b) Yotuel Patient ®

Fig. 4. **Amplitude distribution and material ratio curves after treatment**

ment, curves showed different slopes and different ratios of peaks to valleys.

4. Conclusion

The obtained results show that bleaching treatment has only small effects on surface microhardness of dental enamel. The values remained the same. All measured parameters of surface roughness S_k, S_{pk}, S_{vk} after treatment was changed. The biggest change of surface topography was observed for Yotuel® Patient. In this case, the parameter S_k decreased from 0.426 µm to 0.213 µm. The results show that "in home" bleaching gel with 22 % carbamide peroxide has bigger impact on dental enamel roughness than "in office" bleaching gel with 38 % hydrogen peroxide.

The work presented in this paper has been supported by the institutional development project "Support of Education and Research in Mechanical Engineering" and by the specific research project at the Department of Mechanical Engineering, University of Defence.

REFERENCES

1. Ren Y. F., Amin A., Malmstrom H.: J. Dent. *37*, 6 (2009).
2. Hegedüs C., Bistey T., Flóra-Nagy E., Keszthelyi G., Jenei A.: J. Dent. *27*, 7 (1999).
3. Attin T., et al.: Dental Mater. *25*, 143 (2009).
4. Markovic L., Jordan R. A., Nebojsa L., Gaengler P.: J. Endodontics *33*, 5 (2007).
5. ČSN EN ISO 4287 – Geometrical Product Specifications (GPS) – Surface texture: Profile method -Terms, definitions and surface texture parameters.
6. ISO 25178 – Geometrical product specifications (GPS) – Surface texture: Areal – Part 2: Terms, definitions and surface texture parameters.
7. Ctvrtlik R., Morozova J., Zapletalova Z., Ranc V.: Chem. Listy *105*, s785 (2011).

Q. D. Tran[a], K. Maňas[a], E. Svoboda[a], M. Bumbálek[b], and Z. Joska[a] *([a] Department of Mechanical Engineering, University of Defence in Brno, [b] Department of Dental Care, Faculty of Medicine, Masaryk University):*
Impact of Bleaching Gels on Dental Enamel Microhardness and 3D Surface Roughness

The aim of this study was to characterize the effect of two different bleaching gels (with 22 % carbamide peroxide and with 35 % hydrogen peroxide) on the surface roughness and microhardness of enamel. Bleaching gels were applied according to manufacturer´s instructions. For characterization of surface microhardness and 3D surface roughness, non contact 3D profilometer Talysurf CLI 1000 and Vickers microhardness method were used. The results of surface microhardness did not show significant changes from baseline for both gels. 3D surface roughness parameters showed that "in home" gel with 22 % carbamide peroxide caused bigger changes of enamel topography than "in office" gel with 35 % hydrogen peroxide.